Systematic shell-model study of β-decay properties and Gamow-Teller strength distributions in $A \approx 40$ neutron-rich nuclei

Sota Yoshida,[1,2,*] Yutaka Utsuno,[2,3,†] Noritaka Shimizu,[3] and Takaharu Otsuka[1,3,4,5]

[1]*Department of Physics, the University of Tokyo, Hongo, Bunkyo-ku, Tokyo 113-0033, Japan*
[2]*Advanced Science Research Center, Japan Atomic Energy Agency, Tokai, Ibaraki 319-1195, Japan*
[3]*Center for Nuclear Study, the University of Tokyo, Hongo, Bunkyo-ku, Tokyo 113-0033, Japan*
[4]*RIKEN Nishina Center, 2-1 Hirosawa, Wako, Saitama 351-0198, Japan*
[5]*Instituut voor Kern- en Stralingsfysica, KU Leuven, B-3001 Leuven, Belgium*

(Received 13 March 2018; published 18 May 2018)

We perform large-scale shell-model calculations of β-decay properties for neutron-rich nuclei with $13 \leqslant Z \leqslant 18$ and $22 \leqslant N \leqslant 34$, taking the first-forbidden transitions into account. The natural-parity and unnatural-parity states are calculated in the $0\hbar\omega$ and $1\hbar\omega$ model spaces, respectively, within the full $sd + pf + sdg$ valence shell. The calculated β-decay half-lives and β-delayed neutron emission probabilities show good agreement with the experimental data. The first-forbidden transitions make a non-negligible contribution to the half-lives of $N \gtrsim 28$ nuclei. The low-lying Gamow-Teller strengths of even-even nuclei are considerably larger than those of the neighboring odd-A and odd-odd nuclei, strongly affecting the half-lives and neutron emission probabilities. It is shown that this even-odd effect is caused by the $J^\pi = 1^+$ proton-neutron pairing interaction. We derive a formula to represent the positions of the Gamow-Teller giant resonances from the calculated strength distributions.

DOI: 10.1103/PhysRevC.97.054321

I. INTRODUCTION

The β-decay properties of unstable nuclei have attracted renewed interest with recent experimental progress in exploring the nuclear chart toward the drip line (see [1–6] for examples of recent β-decay measurements performed at several facilities). The β-decay half-lives and the β-delayed neutron emission probabilities of very neutron-rich nuclei are of particular importance for understanding r-process nucleosynthesis. In spite of such experimental developments, most of the nuclei on the r-process path are still not accessible, and reliable theoretical predictions are thus highly in demand.

For calculating β-decay half-lives and β-delayed neutron emission probabilities, β strength distributions are needed, in addition to the $Q(\beta^-)$ values. Among the total β strengths, the Gamow-Teller (GT) strengths are usually of primary importance, whereas the contribution of the first-forbidden (FF) transitions should be considered for the nuclei whose low-lying GT strengths are hindered. Apart from the gross theory for β decay (see [7] and references therein), the microscopic description of the β strength distribution has been developed to cover the whole nuclear chart. The microscopic calculations in this direction are usually based on the quasiparticle random phase approximation (QRPA) [8,9] with some simplifications involved, such as using a separable interaction [8] or assuming spherical shapes [9]. These global calculations are widely used for r-process nucleosynthesis calculations [10]. Very recently, more sophisticated QRPA calculations for even-even nuclei with $28 \leqslant Z \leqslant 110$, $A \geqslant 50$ were reported [11]. Nevertheless, the resulting level of agreement between the calculations of Ref. [11] and experiment is not significantly improved, and the authors of Ref. [11] suggest the need for including correlations beyond QRPA, such as multiphonon effects.

While GT strength distributions are measured for stable nuclei by using charge-exchange reactions [12], those of unstable nuclei are missing, except in a few cases [13–16]. Hence reliable estimates of GT strength distributions in neutron-rich nuclei can be of great help for improving the description of the β-decay properties, even though they cover only a specific region of the nuclear chart.

The shell-model calculation takes full correlations into account within the model space adopted, and is thus successfully applied to systematic studies of GT transitions for the sd shell [17] and for the pf shell [18,19]. On the basis of a good description of the GT strength distributions, shell-model results provide a reliable database for astrophysical purposes [20]. One of the key elements to those successful shell-model calculations of GT transitions is, besides employing well-tested effective interactions, performing the full major-shell calculations which satisfy the GT sum rule. Since the GT operator $\sigma t_\pm$ causes the single-particle transitions not only to the same orbital but also to its spin-orbit partner, the full inclusion of the spin-orbit partners in the model space is crucial. In particular, it is necessary to employ a model space that satisfies the GT sum rule when one investigates the GT strength distribution toward higher excitation energy. For very neutron-rich nuclei, since such complete shell-model calculations are nearly impossible in most cases because of quite different Fermi surfaces for protons and neutrons, relatively small valence shells were taken in previous studies,

*s.yoshida@nt.phys.s.u-tokyo.ac.jp
†utsuno.yutaka@jaea.go.jp

including [21–24]. Full strength distribution is thus out of the scope in such cases.

In the present study, we carry out large-scale shell-model calculations of β-decay half-lives and β-delayed neutron emission probabilities for neutron-rich nuclei with $13 \leqslant Z \leqslant 18$, $22 \leqslant N \leqslant 34$. FF contributions are also taken into account. What is unique in this study is that we obtain GT strength distributions that satisfy the GT sum rule by employing an appropriate model space for this purpose. As a result, on the basis of good agreement with experimental data, we are able to discuss the evolution of the GT strength distribution from stable nuclei to very neutron-rich nuclei, which is beyond the capability of the previous shell-model calculations.

This paper is organized as follows. In Sec. II, the outline of the calculation is presented. In Sec. III, we show the results of β-decay half-lives and β-delayed neutron emission probabilities, and analyze those errors. In Sec. IV, we discuss the systematics of the GT strength distribution, focusing on the odd-even effect of low-lying strengths and on the position of the GT giant resonances. In Sec. V, a summary of the work is provided. Detailed results of the calculations are available in the Supplemental Material for this article [25].

II. OUTLINE OF THE CALCULATION

A. Shell-model calculations

In the present study, we perform large-scale shell-model calculations to investigate β-decay properties for 77 β-unstable nuclei with $13 \leqslant Z \leqslant 18$ and $22 \leqslant N \leqslant 34$. It is reasonable to assume that the ground states of those nuclei are dominated by $0\hbar\omega$ configurations, because we do not consider nuclei in the island of inversion [26], whose ground states are dominated by $2\hbar\omega$ or higher $n\hbar\omega$ configurations. Here the $n\hbar\omega$ configuration stands for the one associated with $n\hbar\omega$ excitation from the lowest configurations in terms of the harmonic-oscillator quantum number. As illustrated in the left panel of Fig. 1, the valence shell for describing those initial states consists of the full sd shell for protons and the pf shell for neutrons; the neutron sd shell is fully occupied.

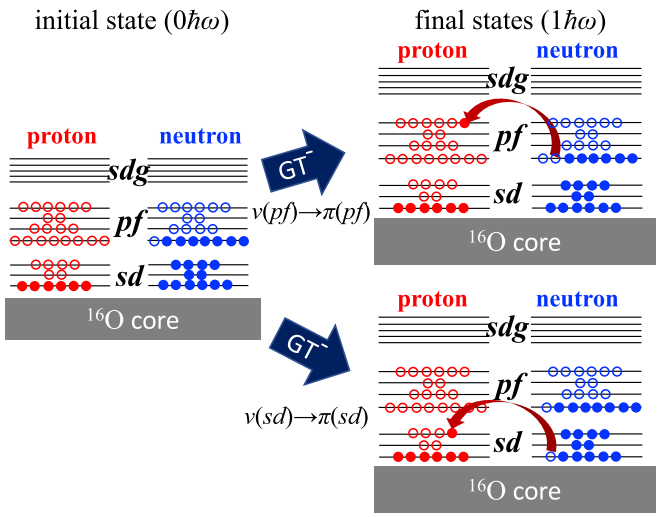

FIG. 1. Schematic illustration of possible GT transitions from a $0\hbar\omega$ configuration. The indices π and ν denote proton and neutron single-particle states, respectively.

Next we consider GT transitions from the $0\hbar\omega$ ground states. As illustrated in Fig. 1, a $\nu(pf) \rightarrow \pi(pf)$ or a $\nu(sd) \rightarrow \pi(sd)$ transition is possible through the GT operator, since the $\sigma t_{\pm}$ operator does not change the quantum numbers n and l. Note that throughout this paper π and ν denote proton and neutron, respectively, except for the case of J^{π} with π being parity. The former and the latter transitions lead to unnatural-parity configurations associated with one-proton excitation and one-neutron excitation from the sd shell to the pf shell, respectively. These configurations, which involve the excitation from the sd shell to the pf shell, are part of the $1\hbar\omega$ configurations. Besides such $1\hbar\omega$ configurations, it is expected that another type of $1\hbar\omega$ configurations that are associated with the excitation from the pf shell to the sdg shell dominate some low-lying unnatural-parity states, especially in $N > 28$ nuclei [27]. Indeed, a recent measurement shows that the $9/2^+_1$ state in ^{49}Ca contains a significant $\nu(1g_{9/2})^1$ component [28]. Although the latter $1\hbar\omega$ configurations are not connected to the ground state through the $\sigma t_{\pm}$ operator, they can be strongly mixed with the former $1\hbar\omega$ states and lower the energies, thus possibly accelerating the GT β decay.

On the basis of the above considerations, concerning GT transitions, we calculate the initial and final states with the full $0\hbar\omega$ and $1\hbar\omega$ basis states, respectively, in the $sd + pf + sdg$ valence shell. The distributions of GT transitions are calculated with the Lanczos strength function method [29,30]. In this study, we carry out 300 Lanczos iterations to obtain converged total half-lives ($T_{1/2}$) and β-delayed neutron emission probabilities (P_n). In addition to GT transitions, we also calculate first-forbidden (FF) transitions as described in Sec. II C. Since the contributions of FF transitions to $T_{1/2}$ and P_n are dominated by those of low-lying levels because of their large Q values, we can restrict ourselves to calculating the lowest 10–20 $0\hbar\omega$ states for estimating the effect of FF transitions. These $0\hbar\omega$ states are calculated with the usual Lanczos diagonalization.

The effective interaction we employ here is the one used in Refs. [27,28]. Its $sd + pf$ shell part is exactly the same as the SDPF-MU interaction [31], and the remaining two-body matrix elements are obtained from a version of the $V_{\rm MU}$ interaction [32] that is adopted in the SDPF-MU interaction. Thus, the present interaction is a natural extension of the SDPF-MU interaction to the $sd + pf + sdg$ valence shell. It should be noted that the SDPF-MU interaction is successful in a systematic description of low-lying level structure in neutron-rich nuclei around $N = 28$ [31].

All the shell-model calculations are performed with the KSHELL code [33]. The maximum M-scheme dimension among the Hamiltonian matrices treated in this study is about 4×10^8.

B. Gamow-Teller transitions

The partial half-life of the GT transition from the initial state i in the parent nucleus to the final state f in the daughter nucleus is expressed as

$$f_0 t^{\rm GT}_{i\rightarrow f} = \frac{K}{(g_A/g_V)^2 B({\rm GT}; i \rightarrow f)}, \quad (1)$$

where K and g_A/g_V are constants, for which we use the values of $K = 6144 \pm 2$ s [9,34] and $g_A/g_V = -1.2701(25)$ [35] throughout this work. The value of f_0 is the Fermi integral which is calculated as

$$f_0 = \int_1^{W_0} F(Z,W)\sqrt{W^2-1}W(W_0-W)^2 dW, \quad (2)$$

where W is the total energy of the emitted electron in units of $m_e c^2$, and $F(Z,W)$ stands for the Fermi function that includes the effect of Coulomb distortion on the electron wave function due to the existence of the nucleus. The W_0 value stands for the maximum W, written as

$$W_0 = Q(\beta^-) + 1 - E_x, \quad (3)$$

where E_x is the excitation energy of the final state f, and $Q(\beta^-)$ denotes the Q value of a given β decay.

The B(GT) value is defined as

$$B(\mathrm{GT}; i \to f) \equiv \frac{1}{2J_i+1}|\langle f||q_{\mathrm{GT}}\sigma t_-||i\rangle|^2, \quad (4)$$

where we follow the convention $t_-|n\rangle = |p\rangle$ and include the quenching factor q_{GT} for the GT operator, which is needed to evaluate the B(GT) value when using shell-model wave functions $|i\rangle$ and $|f\rangle$.

It is well known that the GT strengths satisfy the Gamow-Teller sum rule [36,37] (or the Ikeda sum rule), which is written as

$$S^- - S^+ = 3(N-Z), \quad (5)$$

where $S^\pm$ is defined as

$$S^\pm = \sum_f \frac{1}{2J_i+1}|\langle f||\sigma t_\pm||i\rangle|^2. \quad (6)$$

From the viewpoint of model calculations, the sum rule can be satisfied only when the sum-rule state $\sigma t_\pm|i\rangle$ is completely included in the model space taken. Our calculations satisfy this condition, since the model space for the final states (the full $1\hbar\omega$ space in the $sd + pf + sdg$ valence shell) fully covers the sum-rule state, which is composed of the $1\hbar\omega$ configurations associated with the excitation from the sd shell to the pf shell. In addition, the initial states taken in this study result in $S^+ = 0$ because the $\pi(sd) \to \nu(sd)$ transitions are prohibited due to the Pauli principle. As a result, $S^- = 3(N-Z)$ is satisfied in the present calculations.

The Q value is an important factor to estimate half-lives because f_0 is roughly proportional to Q^5, thus being quite sensitive to it. The $Q(\beta^-)$ value is expressed as

$$Q(\beta^-) = E^{\mathrm{par.}}_{g.s.} - E^{\mathrm{dau.}}_{g.s.} + \delta m, \quad (7)$$

where $E^{\mathrm{par.}}_{g.s.}$ and $E^{\mathrm{dau.}}_{g.s.}$ denote the binding energies of the ground states for the parent and the daughter nuclei, respectively, and δm is given as $\delta m = (m_n - m_p - m_e)c^2 = 0.78$ MeV. Here we take a choice of $E < 0$ for a bound state.

In the shell-model calculations in which the Coulomb force is not included, the binding energy E should be estimated by adding a Coulomb correction term as

$$E = E_{\mathrm{SM}} + E_C(Z,N), \quad (8)$$

where E_{SM} is the binding energy given by the shell-model calculation, and $E_C(Z,N)$ represents the additional Coulomb energy. In this study, $E_C(Z,N)$ is taken from Refs. [38,39]:

$$E_C(Z,N) = 0.700\frac{Z(Z-1) - 0.76[Z(Z-1)]^{2/3}}{R_C}\ \mathrm{MeV}, \quad (9)$$

$$R_C = e^{1.5/A}A^{1/3}\left(0.946 - 0.573\left(\frac{2T}{A}\right)^2\right) \quad (10)$$

with $T = |Z-N|/2$. In the following, the $Q(\beta^-)$ values are taken from experimental data [40] or from the calculations using Eq. (8). In both cases, the excitation energies E_x used in Eq. (3) are taken from the shell-model calculations.

C. First-forbidden transitions

In this study, we also examine the influence of FF transitions on $T_{1/2}$ and P_n by following the formalism of Refs. [41–43]. The partial half-life $t^{\mathrm{FF}}_{i\to f}$ for a given FF transition $i \to f$ is given by

$$f_{\mathrm{FF}} t^{\mathrm{FF}}_{i\to f} = K, \quad (11)$$

where K is the same as the one used for the GT transition [see Eq. (1)], and f_{FF} written as

$$f_{\mathrm{FF}} = \sum_{R=0,1,2} f^{(R)}_{\mathrm{FF}} \quad (12)$$

with $f^{(R)}_{\mathrm{FF}}$ being calculated with the rank-R FF matrix elements as

$$f^{(R)}_{\mathrm{FF}} = \int_1^{W_0} C^{(R)}(W)F(Z,W)\sqrt{W^2-1}W(W_0-W)^2 dW. \quad (13)$$

This expression is similar to f_0 given by Eq. (2), but includes $C^{(R)}(W)$ written as

$$C^{(R)}(W) = \sum_{p=-1,0,1,2} K^{(R)}_i W^p, \quad (14)$$

where nonvanishing $K^{(R)}_i$'s are expressed as

$$\begin{aligned}
\text{rank 0: } & K^{(0)}_{-1} = -\tfrac{2}{3}\mu_1\gamma_1\zeta_0 M^S_0, \\
& K^{(0)}_0 = \zeta_0^2 + \tfrac{1}{9}\left(M^S_0\right)^2, \qquad (15)\\
\text{rank 1: } & K^{(1)}_{-1} = \tfrac{2}{3}\mu_1\gamma_1\zeta_1(x+u), \\
& K^{(1)}_0 = \zeta_1^2 + \tfrac{1}{9}(x+u)^2 - \tfrac{4}{9}\mu_1\gamma_1 u(x+u) \\
& \qquad + \tfrac{1}{18}W_0^2(2x+u)^2 - \tfrac{1}{18}\lambda_2(2x-u)^2, \\
& K^{(1)}_1 = -\tfrac{4}{3}\mu_1 Y - \tfrac{1}{9}W_0(4x^2+5u^2), \\
& K^{(1)}_2 = \tfrac{1}{18}[8u^2 + (2x+u)^2 + \lambda_2(2x-u)^2], \qquad (16)\\
\text{rank 2: } & K^{(2)}_0 = \tfrac{1}{12}z^2\left(W_0^2 - \lambda_2\right), \\
& K^{(2)}_1 = -\tfrac{1}{6}z^2 W_0, \\
& K^{(2)}_2 = \tfrac{1}{12}z^2(1+\lambda_2), \qquad (17)
\end{aligned}$$

TABLE I. Summary of the matrix elements needed for the FF transition with $C = 1/\sqrt{2J_i + 1}$ and $\lambda = -g_A/g_V = +1.2701(25)$ [35]. The fourth column displays the nonrelativistic approximations of M_0^T and $\xi y'$, where M_N is the mass of the nucleon, and E_γ is defined by $E_\gamma = Q(\beta^-) + \Delta E_C - \delta m$ with the Coulomb displacement energy ΔE_C.

Rank		Matrix element (ME)	ME in nonrelativistic approx.
0	M_0^S	$\lambda\sqrt{3}\langle f\|\|ir[C_1 \otimes \boldsymbol{\sigma}]^{(0)}t_-\|\|i\rangle C$	
	M_0^T	$\lambda\sqrt{3}\langle f\|\|\gamma_5 t_-\|\|i\rangle C$	$-\lambda\sqrt{3}\langle f\|\|(i/M_N)[\boldsymbol{\sigma} \otimes \boldsymbol{\nabla}]^{(0)}t_-\|\|i\rangle C$
1	x	$-\langle f\|\|irC_1 t_-\|\|i\rangle C$	
	$\xi' y$	$-\langle f\|\|\boldsymbol{\alpha} t_-\|\|i\rangle C$	$E_\gamma x$
	u	$\lambda\sqrt{2}\langle f\|\|ir[C_1 \otimes \boldsymbol{\sigma}]^{(1)}t_-\|\|i\rangle C$	
2	z	$-2\lambda\langle f\|\|ir[C_1 \otimes \boldsymbol{\sigma}]^{(2)}t_-\|\|i\rangle C$	

with Y, ζ_0 and ζ_1 defined by

$$Y = \xi' y - \xi(u' + x'),$$
$$\zeta_0 = M_0^T + \xi M_0^{S'} + \tfrac{1}{3} M_0^S W_0, \tag{18}$$
$$\zeta_1 = Y + \tfrac{1}{3}(u - x)W_0. \tag{19}$$

In the above expressions, ξ and γ_1 are constants expressed as $\xi = \alpha Z/(2R)$ and $\gamma_1 = \sqrt{1 - (\alpha Z)^2}$ with the fine structure constant α and the charge radius R for a uniform charge distribution. Since μ_1 and λ_2 are known to be very close to unity for light nuclei, we take $\mu_1 = \lambda_2 = 1$ as usually adopted [41]. The remaining quantities M_0^S, M_0^T, x, $\xi' y$, u, and z and their primed values $M_0^{S'}$, x', and u' denote the nuclear matrix elements of the FF operators. The unprimed matrix elements are summarized in Table I. The nonrelativistic forms of M_0^T and $\xi' y$ are used in this study. The primed matrix elements are calculated with the operator multiplied by

$$1 - \frac{1}{5}\left(\frac{r}{R}\right)^2 \quad \text{for } 0 < r < R,$$
$$\frac{R}{r} - \frac{1}{5}\left(\frac{r}{R}\right)^3 \quad \text{for } r > R. \tag{20}$$

D. Effective operators

To obtain the observables that can be compared to experimental data in the shell-model calculations, one should use effective operators in general. For each bare operator $\hat{O}_i$, we use the effective operator expressed as $\hat{O}_i^{\text{eff}} = q_i \hat{O}_i$ with a scaling factor q_i introduced. The scaling factors we take for calculating the GT and FF matrix elements are summarized in Table II. The scaling factor for the GT operator [q_{GT} in Eq. (4)] is taken from a typical value of the pf-shell calculations [44], and the ones for the FF operators are determined to well reproduce the log ft values of FF transitions in neutron-rich K isotopes [45]. Note that these scaling factors are close to the ones used for a previous shell-model study of the FF matrix elements for $A \approx 40$ nuclei [41].

TABLE II. Summary of the scaling factors that define the effective GT and FF operators compared between the present study and Warburton *et al.* [41]. See the text for more details.

	GT	FF				
		M_0^S	M_0^T	x	u	z
present	0.74	1	1.7	1	1	0.55
Ref. [41]		1.1	1.5	1	1	0.51

E. Total half-lives and β-delayed neutron emission probabilities

By using all the partial half-lives of the GT and FF decays, which are given in the previous subsections, the total half-life $T_{1/2}$ is written as

$$\frac{1}{T_{1/2}} = \sum_f \frac{1}{t_{i\to f}}, \tag{21}$$

where f runs over all the possible daughter states that are allowed to be populated through the GT and FF transitions.

To evaluate the β-delayed neutron emission probabilities P_n, we assume that all the β decays to the daughter states f above the one-neutron separation energy S_n lead to neutron emission. The value of P_n is then given by

$$P_n = \left(\sum_{E_f \geqslant S_n} \frac{1}{t_{i\to f}}\right) \Big/ \left(\sum_{\text{all } f} \frac{1}{t_{i\to f}}\right). \tag{22}$$

III. RESULTS OF THE HALF-LIVES AND NEUTRON EMISSION PROBABILITIES

In this section, we compare the calculated $T_{1/2}$ and P_n with available experimental data. After showing an overall comparison of $T_{1/2}$ and P_n in Sec. III A, we provide a quality analysis of the calculated half-lives in Sec. III B.

A. Comparison between theory and experiment

The calculated β-decay half-lives $T_{1/2}$ are compared to the experimental data in Fig. 2. See Tables IV, V and VI shown in the Appendix for their numerical values. Figures 2(a) and 2(b) show the results for the parent nuclei with odd Z and even Z numbers, respectively. Here we take two choices of the $Q(\beta^-)$ values for calculating $T_{1/2}$, i.e., experimental and calculated ones, whose results are presented with the solid and dashed lines, respectively. For both $Q(\beta^-)$ values, overall agreement between experiment and theory is good. An apparent discrepancy is seen only for the $T_{1/2}$ of ^{36}Al ($N = 23$). One possible explanation of this discrepancy may be that the ground state of ^{36}Al is not dominated by the $0\hbar\omega$ configurations, whereas confirming the $T_{1/2}$ data of ^{36}Al by another experiment is also desired because the known $T_{1/2}$

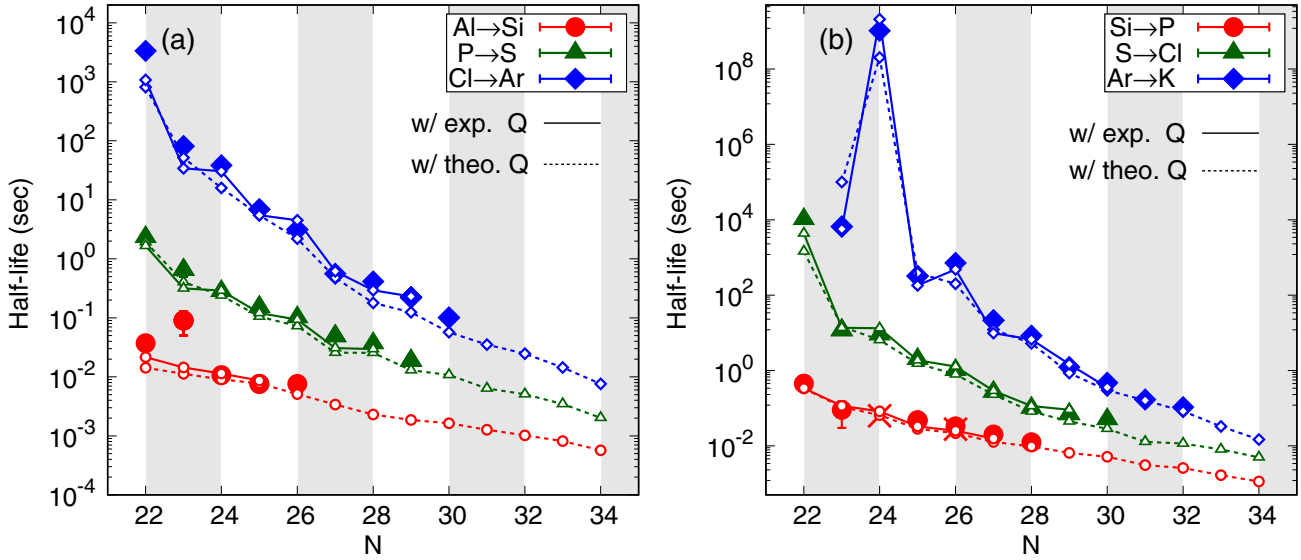

FIG. 2. Comparison of β-decay half-lives between theory and experiment. The panels (a) and (b) correspond to β decays from odd-Z and even-Z isotopes, respectively. The filled symbols and cross symbols (^{38,40}Si) denote the experimental data taken from the ENSDF database [46] and a recent measurement [47], respectively. The open symbols connected by the solid and dashed lines stand for our results calculated with the experimental and calculated $Q(\beta^-)$ values, respectively.

value in ^{36}Al is much longer than those of the neighboring Al isotopes.

Here we examine the effects of the first-forbidden (FF) transitions on the half-lives by comparing the $T_{1/2}$ values with and without the FF transitions included. Figure 3 shows the ratio of the half-lives with FF to the ones without FF. If this ratio is close to 100%, the FF transitions are negligible. We predict that on the whole the contributions of the FF transitions are enhanced with increasing neutron number. In particular, the partial half-lives of the FF transitions are comparable to those of the GT transitions for Si and P isotopes with $N \approx 34$.

This overall behavior is partly due to the following properties which suppress low-lying GT strengths with increasing neutron number N. First, the calculated excitation energies of the lowest unnatural-parity states gradually increase with N. Second, as we will discuss in more detail in Sec. IV, the GT

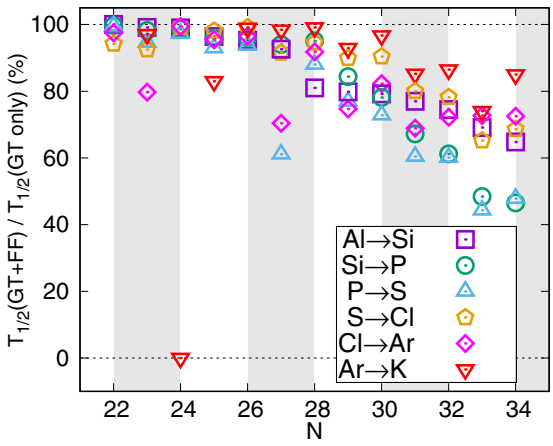

FIG. 3. Ratio of the half-life with the FF transitions included to the one without the FF transitions included.

giant resonance (GTGR) well develops at higher excitation energies for larger N, hence considerably depleting low-lying GT strengths. Although the first property may be specific to this particular mass region, it is most likely that the second one can be rather universal in the whole nuclear chart.

For the $N \gtrsim 28$ nuclei we study, some low-lying FF matrix elements are enlarged, thus contributing substantially to the total half-lives. This is dominated by the neutron Fermi surface moving to the $2p$ orbitals. If the valence neutrons were completely confined in the $1f_{7/2}$ orbital, only the $\nu 1f_{7/2} \rightarrow \pi 1d_{5/2}$ FF transition with $\Delta J^\pi = 1^-$ and the $\nu 1f_{7/2} \rightarrow \pi 1d_{3/2}$ FF transition with $\Delta J^\pi = 2^-$ would be possible, hence no $\Delta J^\pi = 0^-$ FF transitions would take place. The $\Delta J^\pi = 0^-$ FF transition, which occurs with the neutron $2p$ orbitals occupied, can bring about a small log ft value, as is known for the ^{50}K$(0^-) \rightarrow {}^{50}Ca(0^+)$ β decay [48] dominated by the $\nu 2p_{3/2} \rightarrow \pi 1d_{3/2}$ single-particle transition. The $\Delta J^\pi = 0^-$ FF transition has also a large impact on the $T_{1/2}$ values of the $N = 27$ isotones ^{42}P and ^{44}Cl, as shown in Fig. 3. Although they have only 27 neutrons, their last neutron carries a large $2p_{3/2}$ component because of the breaking of the $N = 28$ closure in neutron-rich nuclei.

It should be noted that the β^- decay of ^{42}Ar is caused only by the FF transitions because no unnatural-parity states are located in the $Q(\beta^-)$ window.

For some neutron-rich nuclei with $N \leqslant 28$, β-decay half-lives and Gamow-Teller strength distributions were calculated in previous shell-model studies [47,49–51], where the sdg orbitals are omitted from the valence shell and the FF transitions are not taken into account. If the sdg orbitals are removed in the present study, GT-decay half-lives are enlarged by $\sim$30% at most. Hence, considering minor contributions of the FF transitions for $N \leqslant 28$ nuclei as presented in Fig. 3, we confirm that those previous calculations provide reasonable estimates of half-lives.

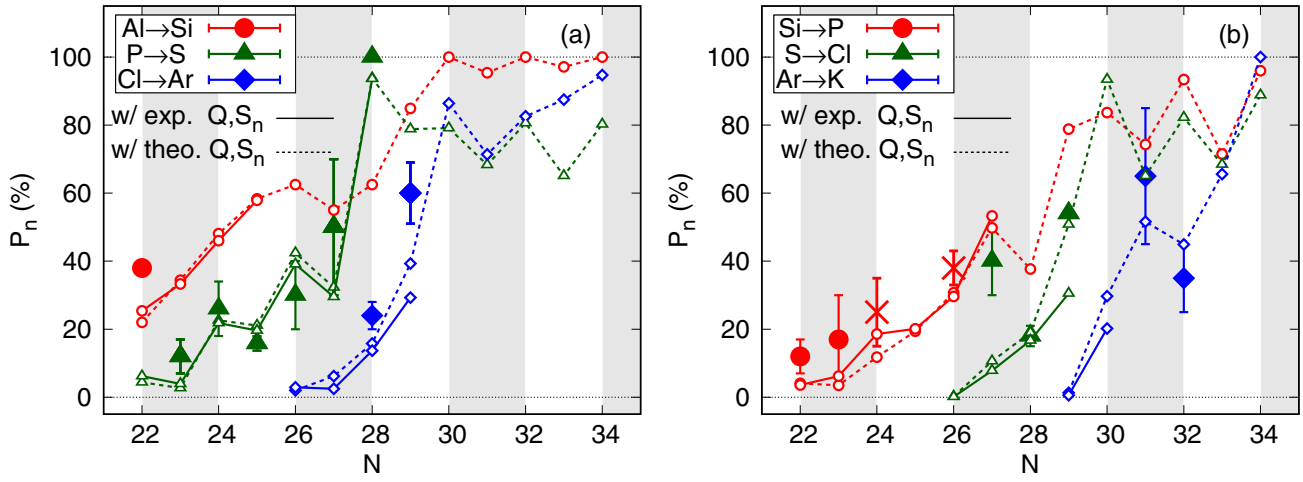

FIG. 4. Comparison of β-delayed neutron emission probabilities P_n between theory and experiment. The meanings of the symbols and the lines are the same as in Fig. 2.

Now we move on to the β-delayed neutron emission probability P_n. This quantity provides a stringent test for the distribution of B(GT) strengths in the low-lying energy region, especially when the S_n value of the daughter nucleus is less than ~5 MeV. In Fig. 4, the calculated P_n values are compared to the experimental data. The present calculations well reproduce the experimental data, while the number of available data is limited and some of the measured values have large uncertainties.

From Fig. 4, while the P_n value generally increases with increasing neutron number as expected, clear odd-even staggering can also be seen. This staggering is supported by the experimental systematics of β decays of P isotopes, where the P_n value of an odd-N parent nucleus is smaller than the mean value of its neighboring even-N nuclei. Such odd-even staggering is known in other regions, e.g., for ^{82,83,84}Ga, whose P_n values were measured very recently [52]. This feature is basically understood in terms of pairing correlation which causes the odd-even dependence of the size of the $Q(\beta^- n)$ window, i.e., the range of excitation energy above S_n and below $Q(\beta^-)$, compared to that of the $Q(\beta^-)$ window. As an example, we now pick up the β decays of ^{42}P ($N = 27$) and ^{43}P ($N = 28$), whose measured P_n values are 50(20)% and 100%, respectively [46]. The former decay has $Q(\beta^-) = 18.65(31)$ MeV and $S_n = 6.700(5)$ MeV, while the latter decay has $Q(\beta^-) = 16.88(55)$ MeV and $S_n = 2.629(6)$ MeV [40]. This enlarged $Q(\beta^- n)$ window in the β decay of ^{43}P is in good accordance with the enhanced P_n value.

Very interestingly, there are a few cases that follow the opposite odd-even dependence in P_n. One case that is supported by both experiment and theory is the β decays of ^{49}Ar ($N = 31$) and ^{50}Ar ($N = 32$), whose adopted P_n values in the ENSDF database are $P_n = 65(20)\%$ and $P_n = 35(10)\%$, respectively.[1] This property cannot be explained by the size of the $Q(\beta^- n)$ window, and should be related to the difference in GT strength distribution between those two nuclei. Further discussions on this will be given in Sec. IV.

B. Error analysis

In this subsection, we analyze the errors of the calculated half-lives $T_{1/2}$ more quantitatively. One usually uses $T_{1/2}^{\rm calc} - T_{1/2}^{\rm exp}$ as a measure of deviation, where $T_{1/2}^{\rm calc}$ and $T_{1/2}^{\rm exp}$ denote the calculated and experimental $T_{1/2}$ values, respectively. For the present purpose, however, this quantity is not suitable because the $T_{1/2}$ value ranges over orders of magnitude, hence errors for large $T_{1/2}$ values are magnified. To treat the $T_{1/2}$ values of different orders on the same footing, we introduce

$$r = \log_{10}\left(T_{1/2}^{\rm calc}/T_{1/2}^{\rm exp}\right) \tag{23}$$

as a measure of deviation, following the analyses of Refs. [8,9]. Its mean value and standard deviation are expressed as

$$\bar{r} = \frac{1}{n}\sum_{i=1}^{n} r_i \tag{24}$$

and

$$\sigma = \left[\frac{1}{n}\sum_{i=1}^{n}(r_i - \bar{r})^2\right]^{1/2}, \tag{25}$$

respectively, where r_i is r indexed by i. The values $\bar{r}$ and σ represent, respectively, the mean deviation from the experimental data and the mean fluctuation expressed in terms of $\log_{10}$. We also use $10^{\bar{r}}$ and 10^{σ} to express these values in terms of the ratio of the experimental and calculated values. Naturally, $\bar{r} = 0$ and $\sigma = 0$ (or equivalently, $10^{\bar{r}} = 1$ and $10^{\sigma} = 1$) are obtained in the ideal case that all of the calculated values are identical with the experimental values.

Table III shows $\bar{r}$ and σ obtained with our shell-model calculations, together with the corresponding $10^{\bar{r}}$ and 10^{σ}. The discrepancies of the calculated half-lives come from the $Q(\beta^-)$ values and the GT strengths. To extract the errors of the latter origin, we first consider the result using the experimental

[1]The P_n values of the ^{49}Ar and ^{50}Ar β decays were recently remeasured to be 29(6)% and 37(7)%, respectively [53]. Although the opposite odd-even staggering is not seen here, these values are still inconsistent with the normal odd-even staggering mentioned above.

TABLE III. Discrepancies of calculated $T_{1/2}$ values [see Eqs. (24) and (25)], comparing our calculations and the FRDM-QRPA calculations of Möller *et al.* [8]. Concerning this work, the results with the theoretical and and experimental $Q(\beta^-)$ values are presented. In the region of current interest, the half-lives are measured for 47 nuclei, among which the $Q(\beta^-)$ values are known for 40 nuclei.

	This work		Ref. [8]
	Q (theory)	Q (exp.)	
$\bar{r}$	−0.18	−0.09	−0.07
σ	0.29	0.20	0.48
$10^{\bar{r}}$	0.66	0.81	0.85
10^{σ}	1.95	1.58	3.04
n	47	40	47

$Q(\beta^-)$ values. The obtained $\bar{r}$ is −0.09, representing that the mean value of the calculated half-lives is 81% of that of the experimental ones. If the quenching factor $q_{\rm GT} = 0.67$ is used instead of $q_{\rm GT} = 0.74$, which is employed in this study, this difference disappears. Although it is not clear whether the negative $\bar{r}$ value is solely due to the quenching factor, $q_{\rm GT} = 0.67$ seems to be within the acceptable range of $q_{\rm GT}$. The σ value is also an important measure of the quality of calculation, partly because it cannot be changed by the choice of $q_{\rm GT}$. The obtained value $\sigma = 0.20$, or $10^{\sigma} = 1.58$, indicates that the present calculations well describe the GT strength distribution on the whole.

Next, we discuss the discrepancies of the half-lives obtained with the calculated $Q(\beta^-)$ values. Table III shows that the σ value slightly increases but is still smaller than that of the QRPA (GT) + gross theory (FF) calculations [8], which are frequently used for providing nuclear input in r-process calculations. Since our calculations probably provide higher predictive power on the basis of better agreement with experiment, it would be interesting to use our half-lives of $13 \leqslant Z \leqslant 18$ nuclei for astrophysical purposes.

As shown in Table III, the $\bar{r}$ value becomes smaller by 0.09 by replacing the experimental $Q(\beta^-)$ values with the calculated ones. This means that the ratio of the half-lives obtained with the calculated $Q(\beta^-)$ values to those of the experimental ones is 0.81 on average, suggesting a systematic deviation in the calculated $Q(\beta^-)$ values. In Fig. 5, the calculated $Q(\beta^-)$ values are compared with the experimental ones, and also with the estimated values by AME2016 [40] if available. The experimental $Q(\beta^-)$ values are well reproduced by the calculations: typical errors are 0.5 MeV or less. Nevertheless, the overall $Q(\beta^-)$ values are slightly overestimated, thus causing shorter half-lives through Q^{-5} sensitivity.

It should be noted that some of the unmeasured $Q(\beta^-)$ values are quite different between our calculations and the AME2016 evaluation [40], as shown in Fig. 5. In particular, the difference for ^{42}Al ($N = 29$) reaches approximately 3.5 MeV. As a result, unlike the calculations with our $Q(\beta^-)$ values, the $T_{1/2}$ values estimated with the AME2016 $Q(\beta^-)$ values exhibit an upward kink at $N = 29$ along the Al isotope chain. In other words, the masses of very neutron-rich nuclei in this region can be probed without direct mass measurement by measuring the half-lives under the assumption that the GT strength distributions are well described by the present shell-model calculations.

IV. DISTRIBUTION OF GAMOW-TELLER STRENGTHS

As shown in the previous section, the present shell-model calculations satisfactorily reproduce experimental half-lives and β-delayed neutron emission probabilities. Since they are dominated by GT transitions, it is considered that our calculations systematically well describe the distributions of GT strengths, which are usually quite difficult to obtain in experiment for very neutron-rich nuclei. In this section, we provide more detailed analyses of the distributions of GT strengths on the basis of our calculations. Although this study is devoted only to a specific mass region, some of the characteristics presented here can be universal and may be applicable to other neutron-rich nuclei.

A. Overall properties

We first survey how the GT strength distribution evolves with increasing neutron number N, taking the Ar → K transitions as an example. The results are summarized in Fig. 6. One can clearly see the development of a large, clear, single peak,

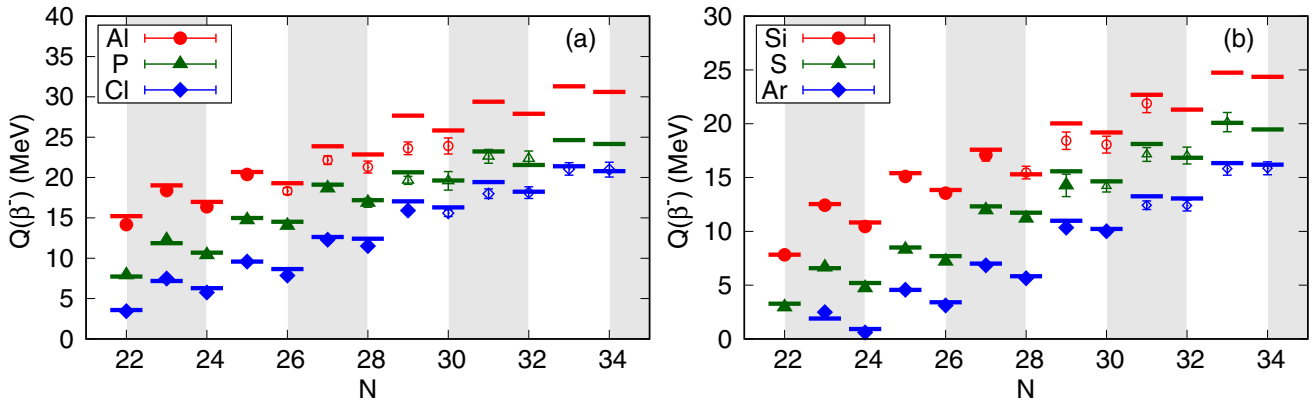

FIG. 5. Comparison of the $Q(\beta^-)$ values between theory and experiment. The filled and open symbols denote the experimental and estimated $Q(\beta^-)$ values taken from the AME2016 [40] database, and the horizontal bars represent our calculated $Q(\beta^-)$ values.

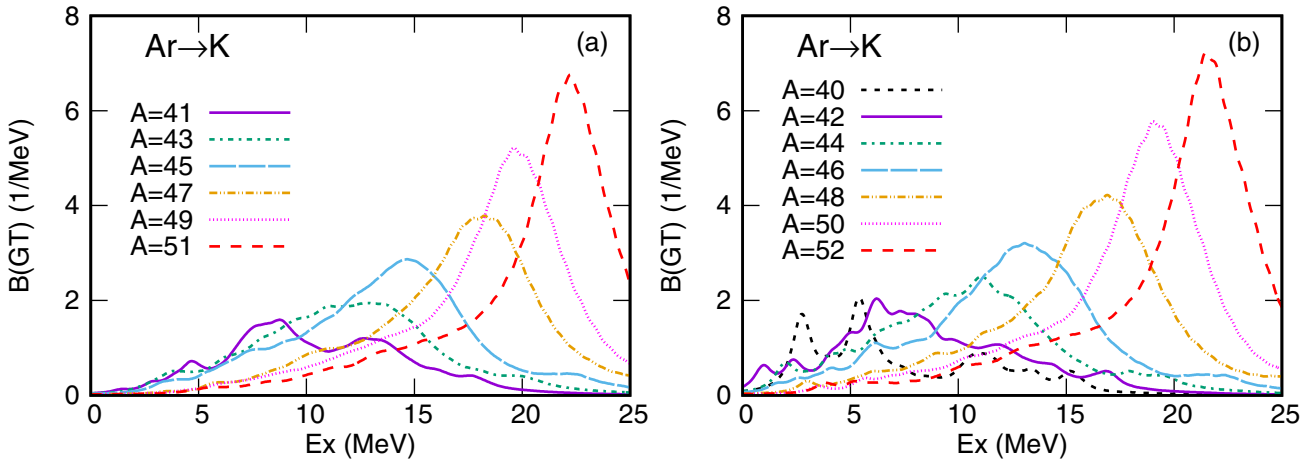

FIG. 6. Evolution of B(GT) distributions in Ar → K transitions. The panels (a) and (b) show the results of odd-A and even-A nuclei, respectively. The strengths are folded with a Lorentzian function with the width parameter $\Gamma = 0.5$ MeV.

which is called Gamow-Teller giant resonance (GTGR), with increasing N. Here, the total B(GT) value increases to satisfy the GT sum rule of Eq. (5), and the peak of the GTGR moves to higher energy. Although the total B(GT) value increases with N, the low-lying strengths, i.e., those of typically below $E_x \lesssim 5$ MeV, decrease. This happens because the GTGR exhausts most of the sum-rule value with its development toward larger N. Since low-lying GT strengths are of greater importance in the half-lives, their decrease leads to an enhanced FF fraction in the β-decay rate as stressed in Sec. III A.

B. Low-energy GT strengths

In this subsection, we concentrate on low-energy GT strengths, which play a crucial role in the total half-lives and β-delayed neutron emission probabilities. In Fig. 7, the low-energy part of Fig. 6 is enlarged. By comparing the smoothed B(GT) distributions between Figs. 7(a) and 7(b), one can immediately find that low-energy GT strengths are stronger in even-A isotopes than in their neighboring odd-A isotopes. In order to get a deeper insight into this even-odd effect, we define a *strong low-energy GT transition* as the one to a discrete level below $E_x = 5$ MeV that has B(GT) > 0.10, which corresponds to $\log ft < 4.58$. All the strong low-energy GT transitions are also drawn in Fig. 7 by the vertical bars. Since there is only one strong low-energy GT transition for odd-A Ar isotopes, the even-odd effect is due to the occurrence of the strong low-energy GT transitions in even-even isotopes.

By applying this analysis to the whole region of the present study, the parent nuclei that have the strong low-energy GT transitions are marked in Fig. 8. Very interestingly, most of even-even nuclei have strong low-energy GT transitions, while odd-A and odd-odd nuclei do not have them, except ^{35,36}Al, ^{37}P, and ^{41}Ar. Note that ^{35,36}Al, ^{37}P, and ^{41}Ar have a single GT transition below $E_x = 5$ MeV with the log ft value slightly smaller than 4.58. For Ar isotopes, all the even-even isotopes calculated in this study have strong low-energy GT transitions. In contrast, no strong GT transitions are predicted for ^{48}Si and ^{48,50}S. This is because low-lying GT strengths are absorbed by the GTGR when it develops with increasing N. With a clear systematics predicted in Fig. 8, this even-odd effect may be

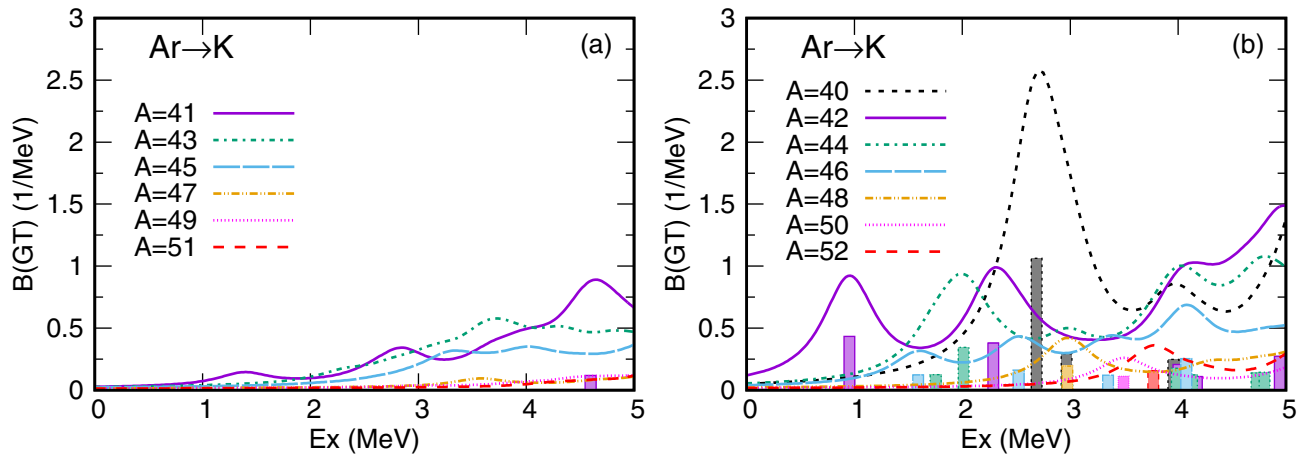

FIG. 7. Same as Fig. 6 but highlighting the excitation energy below 5 MeV. The width parameter Γ is set to 0.3 MeV. The vertical bars indicate discrete levels with B(GT) > 0.10, which corresponds to log $ft \lesssim 4.58$.

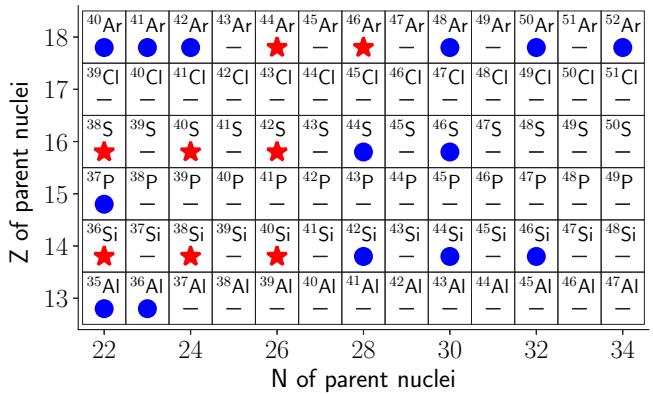

FIG. 8. Illustration of the occurrence of the strong low-energy GT transitions in the region of the present study. The nuclei marked with the red stars indicate that the strong low-energy GT transitions, defined as the ones with $B(\mathrm{GT}) > 0.10$ and $E_x < 5$ MeV, are obtained both in theory and experiment, and the ones with the blue circles denote that the strong low-energy GT transitions are predicted in theory but that no GT strengths are available experimentally. The others have no strong GT transitions either in theory or in experiment.

a rather universal phenomenon in neutron-rich nuclei with N not too far from β stability.

The even-odd effect of low-energy GT transitions can be probed with the experimental data. In Fig. 9, the distributions of the log ft values are compared between experiment and theory for some of the $A \approx 40$ isotopes in which log ft values are available. Here we pick up the β-decay schemes of the ^{39}S, ^{40}S, ^{40}P, and ^{41}Cl parent nuclei as examples of odd-even, even-even, odd-odd, and odd-even isotopes, respectively. Our calculations well reproduce the measured β-decay schemes. For the decays from odd-A and even-even isotopes, unnatural-parity states appear from $E_x \sim$ 1–2 MeV in common, and there are a number of excited states predicted below $E_x = 5$ MeV that can be directly populated via GT transitions. Nevertheless, only the β decay from ^{40}S has a strong low-energy GT transition to the 1^+ level at 2.3 MeV with log $ft = 3.7$, in good agreement with the calculated 1^+ level at 2.1 MeV having log $ft = 3.8$. Similar strong low-energy GT transitions were recently observed in the β decays of ^{38,40}Si ($N = 24$ and 26), and they are well reproduced by our calculations [47].

Once the even-odd effect of low-energy GT transitions is thus established, our interest is directed to the mechanism of causing such strong low-energy GT transitions from the even-even parent nuclei alone. A possible factor that should be considered is the even-odd dependence of the GTGR energies. More detailed discussions are provided in Sec. IV C regarding $E_{\mathrm{GT}} - E_{\mathrm{IAS}}$, which is well described with a smooth function of mass number and isospin, where E_{GT} and E_{IAS} are the excitation energies of the GTGR and the isobaric analog state, respectively. Since E_{IAS} has a strong even-odd dependence originating from pairing correlation, E_{GT} has also a strong even-odd dependence. In fact, the calculated E_{GT} values, which are defined as the energy of the sum-rule state (see

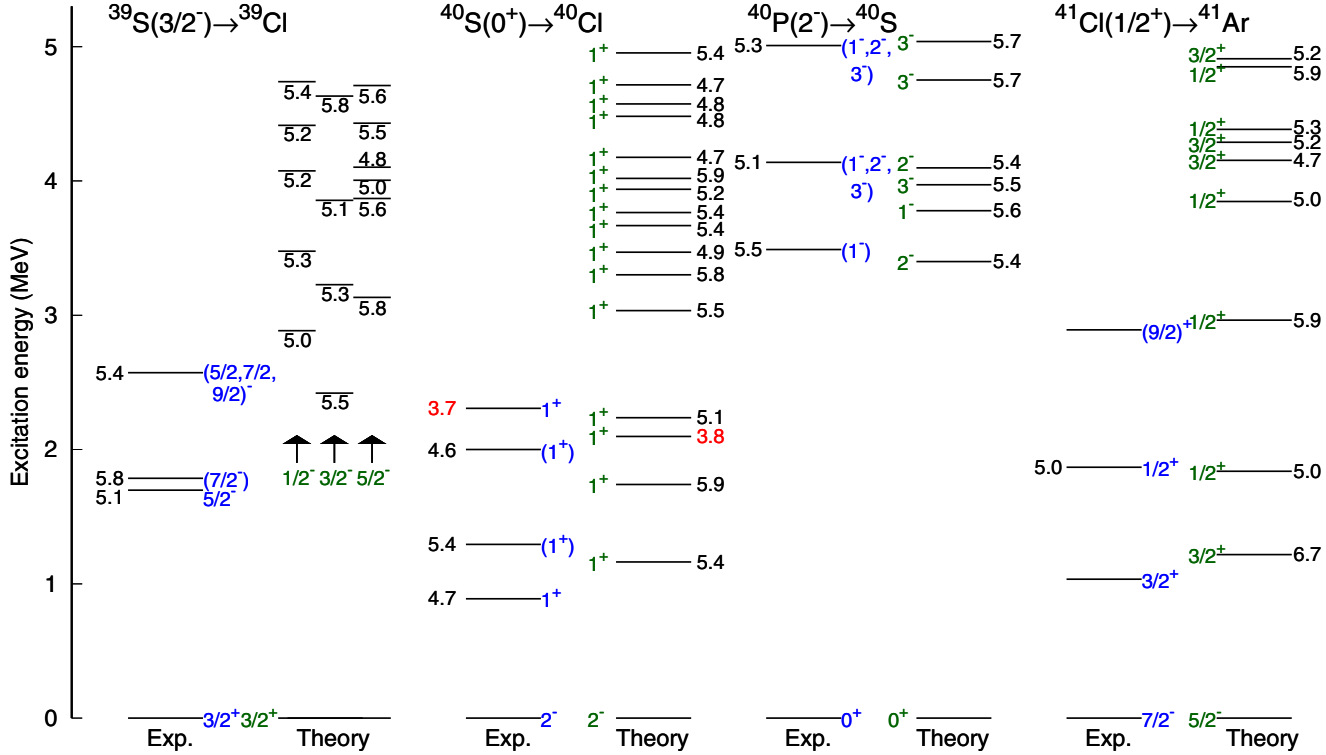

FIG. 9. Low-lying distribution of log ft values for the GT β decays of ^{39}S, ^{40}S, ^{40}P, and ^{41}Cl, comparing experiment and theory. The log ft values are shown near the levels. The experimental data are taken from Ref. [54] for ^{39}S, Ref. [55] for ^{40}S, Ref. [56] for ^{40}P, and Refs. [57–59] for ^{41}Cl. In the calculated energy levels, the states with log $ft \geqslant 6.0$ are omitted except the $3/2^+_1$ state in ^{41}Ar. The calculated levels in ^{39}Cl are arranged according to spin for better visibility.

Sec. IV C), are 10.5, 8.6, 11.9, 10.4, 14.0, 12.6, 17.3, 15.9, 18.8, 18.2, 21.1, and 20.3 MeV for the transitions of $^{41-52}$Ar, respectively. Namely, when the GT transitions are compared between ^{A}Ar and $^{A+1}$Ar with odd A (such as ^{41}Ar vs ^{42}Ar), the latter even-even Ar isotopes have the GTGR located lower by 0.6–1.9 MeV. Hence, the influence of the GTGR on low-energy GT strengths is more significant in even-even isotopes. This mechanism should work, but cannot fully account for the even-odd effect. When the low-energy GT strengths shown in Fig. 6 are compared, for instance, between ^{47}Ar and ^{52}Ar, only the latter has a strong low-energy GT transition in spite of having a larger GTGR energy.

We shall look into nuclear-structure effects in more depth. The strong low-energy GT transitions are characterized as the occurrence of low-lying discrete 1^+ states in odd-odd nuclei that have large B(GT) values from the 0^+ ground states of even-even nuclei. The spin-isospin component of the NN interaction may favor proton-neutron pairs in the daughter nucleus, created by action of the GT operator on a BCS-type neutron-neutron pair contained in the ground state of the parent nucleus. This expectation can be incorporated into actual calculations. In fact, in the case of the QRPA, it is recognized that the inclusion of the proton-neutron pairing interaction significantly shortens the half-lives by pulling GT strengths to lower energy [60] (see also [61,62] for recent works). The effect of the proton-neutron pairing interaction on the GT distribution in $N \approx Z$ nuclei was recently investigated in depth in Refs. [63,64], which showed clear enhancement of low-energy GT strengths with the proton-neutron pairing interaction taken into account and hence well reproduced recent experimental data [65]. Bearing those previous studies in mind, here we examine the effect of the proton-neutron 1^+ pairing terms on the development of the strong low-energy GT transitions. For this purpose, GT strength distributions are calculated by switching off the Hamiltonian matrix elements with a proton and a neutron coupled to $J^\pi = 1^+$, and the results are compared to the ones obtained with the original interaction. More specifically, all the $\langle a_\pi b_\nu J^\pi | V | c_\pi d_\nu J^\pi \rangle$ matrix elements with $J^\pi = 1^+$ are set to zero. In addition, to minimize the side effect of changing the interaction, the diagonal matrix elements $\langle a_\pi b_\nu J^\pi | V | a_\pi b_\nu J^\pi \rangle$ are shifted by $\Delta V_{ab}^{\mathrm{m},pn}$, where $\Delta V_{ab}^{\mathrm{m},pn}$ is determined so that the monopole matrix elements $V_{ab}^{\mathrm{m},pn} \equiv \sum_J (2J+1)\langle a_\pi b_\nu J | V | a_\pi b_\nu J \rangle / \sum_J (2J+1)$ can be the same as those of the original interaction. This change of the interaction does not affect the $0\hbar\omega$ states considered in this study, in which active protons and neutrons reside only in the sd shell and in the pf shell, respectively. Hence all the initial states are kept unchanged, so are the $Q(\beta^-)$ values and the neutron separation energies. Namely, we now extract the role of the 1^+ proton-neutron pairing in the GT strength distribution through the changing nuclear structure in the daughter nucleus.

Here we take the GT strengths of ^{50}Ar as an example. As discussed in Sec. III A, the P_n value of the β decay from this nucleus seems to be quite small compared to the systematics, and it is interesting to investigate its low-energy GT strengths. The result is shown in Fig. 10. As depicted in the inset of Fig. 10, the small P_n value is accounted for by a strong GT transition to the 1^+ state located at 3.5 MeV with B(GT) = 0.11. When the proton-neutron 1^+ pairing matrix

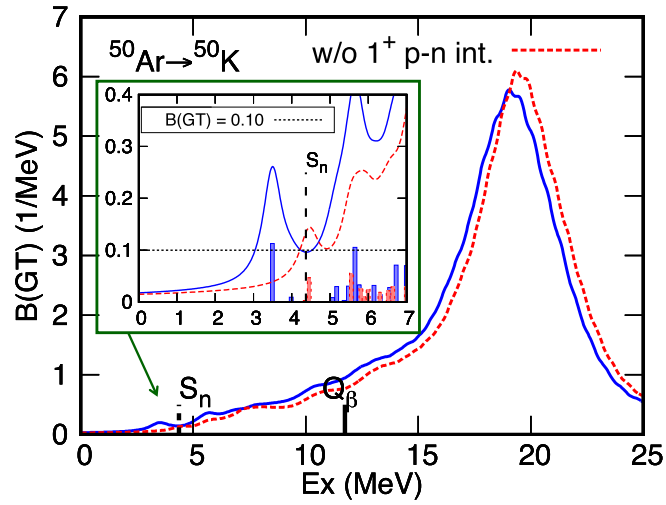

FIG. 10. B(GT) distribution in ^{50}Ar, comparing the calculations with (solid lines) and without (dashed lines) the proton-neutron pairing matrix elements. The strengths are folded in the same way as in Figs. 6 and 7. See the text for more details.

elements are switched off in the way described above, the shape of the GTGR is almost the same and its position is shifted slightly higher. On the other hand, the effect on low-energy GT transitions is remarkable, as shown in the inset of Fig. 10. Similarly to the GTGR, their positions are shifted higher, but their strengths are reduced almost by half. As a result, the even-odd effect of the low-energy GT strengths is much less pronounced. It is quite interesting to see that the proton-neutron pairing interaction is still quite effective in very neutron-rich nuclei whose Fermi surfaces for protons and neutrons are located in different major shells.

C. Position of the Gamow-Teller giant resonance

As shown in Fig. 6, the GTGR develops with increasing neutron number, and the overall GT strength distribution is well approximated by a simple function similar to the giant dipole resonances. One of the most important properties of the GTGR is its position. The position of the GTGR is also practically important as a main input of the gross theory for β decay [66]. In this subsection, we deduce the systematics of the position of the GTGR from the calculated strength distribution.

The position of the GTGR, E_{GT}, is usually written as the difference from the position of the isobaric analog state (IAS), E_{IAS}. It is pointed out in Ref. [67] that $E_{\mathrm{GT}} - E_{\mathrm{IAS}}$ is approximately proportional to $T_0 A^{-1}$, with $T_0 = (N-Z)/2$ in the absence of spin-orbit splitting. On the basis of this argument, two different empirical formulas of $E_{\mathrm{GT}} - E_{\mathrm{IAS}}$ are proposed:

$$E_{\mathrm{GT}} - E_{\mathrm{IAS}} = 6.7 - 60 T_0 A^{-1}\ \mathrm{MeV} \tag{26}$$

in Ref. [68] or

$$E_{\mathrm{GT}} - E_{\mathrm{IAS}} = 26 A^{-1/3} - 37 T_0 A^{-1}\ \mathrm{MeV} \tag{27}$$

in Ref. [69]. These empirical formulas are constructed to fit experimental GTGR energies deduced from the (p,n) reaction data for several β-stable nuclei with A = 90–200 and

$(N-Z)/A = 0.10$–0.22. Since the isospin dependent terms in Eqs. (26) and (27) differ by a factor of 1.6, those two formulas predict rather different $E_{\rm GT}$ values for very neutron-rich nuclei. However, they cannot be discriminated by using only the available data due to the lack of experimental information on unstable nuclei. It is thus of great interest and importance to examine what isospin dependence is realized for very neutron-rich nuclei on the basis of the present calculations that well reproduce experimental β-decay properties. The present study covers a wide range of neutron richness, with $(N-Z)/A$ ranging from 0.10 to 0.45 in a small mass region, thus more directly extracting isospin dependence.

In this study, the position of the GTGR is defined as the centroid of the B(GT) values. Namely it is expressed as

$$E_{\rm GT} = \frac{m_1({\rm GT}^-)}{m_0({\rm GT}^-)}, \tag{28}$$

where $m_k({\rm GT}^-)$ denotes the kth moment of the GT strength distribution written as

$$m_k({\rm GT}^-) = \sum_f [E_x(f)]^k B({\rm GT}^-; i \to f). \tag{29}$$

This provides a unique definition of $E_{\rm GT}$ in theory, whereas there is some ambiguity if one extracts $E_{\rm GT}$ from the peak energy of the B(GT) distribution, especially when the GTGR is not well developed in less neutron-rich nuclei. In the present calculations, the centroid energy is smaller than the peak energy of the main GTGR peak by up to $\sim$1 MeV because the tails of the GTGR are more extended to the low-energy side than to the high-energy side, as known experimentally, for instance, from Ref. [70]. Note that $E_{\rm IAS}$ is easily identified in the shell model because of isospin conservation.

Using the $E_{\rm GT} - E_{\rm IAS}$ values thus obtained, we deduce a formula to fit those data. Following Eqs. (26) and (27), here we assume two functional forms, $E_{\rm GT} - E_{\rm IAS} = C_1 + C_2 T_0 A^{-1}$ MeV and $E_{\rm GT} - E_{\rm IAS} = C_1' A^{-1/3} + C_2' T_0 A^{-1}$ MeV, and determine the parameters (C_1, C_2) and (C_1', C_2') with a least-squares fit. As a result, we get

$$E_{\rm GT} - E_{\rm IAS} = 5.1 - 40 T_0 A^{-1}\ {\rm MeV} \tag{30}$$

for the form $C_1 + C_2 T_0 A^{-1}$ and

$$E_{\rm GT} - E_{\rm IAS} = 17 A^{-1/3} - 38 T_0 A^{-1}\ {\rm MeV} \tag{31}$$

for the form $C_1' A^{-1/3} + C_2' T_0 A^{-1}$. We then examine how well these formulas account for the calculated $E_{\rm GT} - E_{\rm IAS}$ values. In Fig. 11, we plot the systematics versus shell model for $E_{\rm GT} - E_{\rm IAS}$. The strong correlation shown in Fig. 11 indicates that the shell-model values are well represented by the systematics of Eqs. (30) and (31). As shown in the insets of Fig. 11, the standard deviations of those formula are only a few hundred keV. The isospin-dependent terms of Eqs. (30) and (31) are rather similar, since only a small mass region is considered now. The resulting isospin dependence supports that of Eq. (27). On the other hand, the first terms of Eqs. (30) and (31) are smaller than those of Eqs. (26) and (27).

One of the interesting features in the present shell-model results shown in Fig. 11 is that the GTGR energy can be lower than the IAS energy, i.e., $E_{\rm GT} - E_{\rm IAS} < 0$ for very neutron-rich nuclei. Although this is predicted by the systematics that shows linear dependence on T_0, all the available experimental data exhibit $E_{\rm GT} - E_{\rm IAS} > 0$. Moreover, the systematics of the (^{3}He,t) reaction data in $^{112-124}$Sn suggests that the $E_{\rm GT} - E_{\rm IAS}$ value appears not to linearly decrease with increasing N but to asymptotically approach zero [70]. We stress that those data are limited to β-stable nuclei with small neutron excess, and hence $E_{\rm GT} - E_{\rm IAS} < 0$ is not realized. It is thus very interesting to measure the evolution of $E_{\rm GT} - E_{\rm IAS}$ toward very neutron-rich nuclei using radioactive isotope beams.

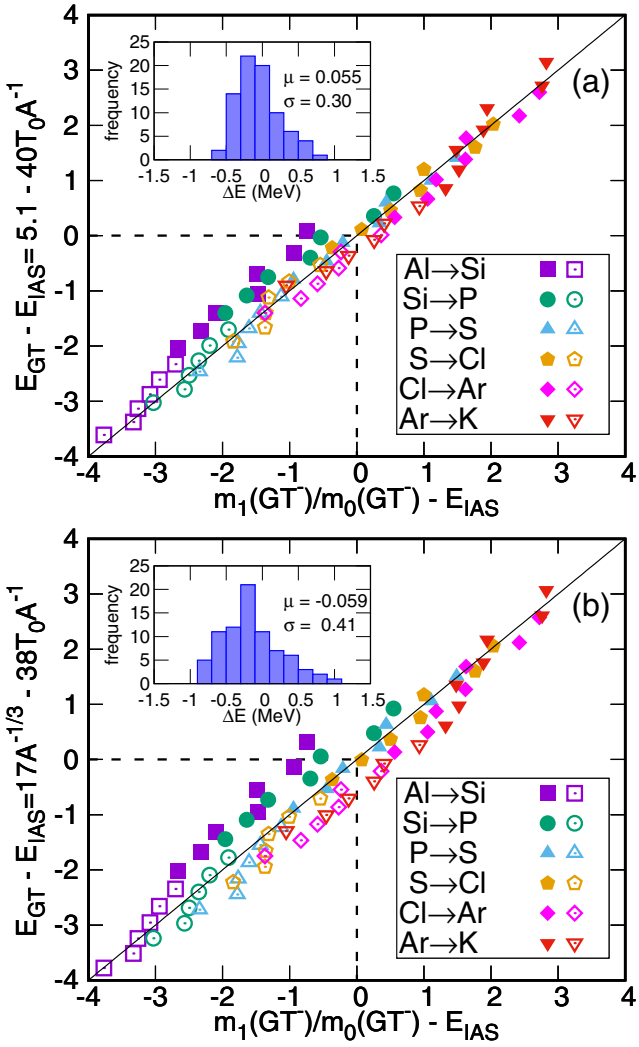

FIG. 11. Systematics (vertical axes) versus shell model (horizontal axes) for the $E_{\rm GT} - E_{\rm IAS}$ value. In panels (a) and (b), respectively, Eqs. (30) and (31) are used for the systematics. Filled and open symbols correspond to the parent nuclei with $N \leqslant 28$ and $N > 28$, respectively. The insets show the distribution of the deviation of $E_{\rm GT} - E_{\rm IAS}$ estimated by those systematics, together with the mean value μ and the standard deviation σ.

The position of the GTGR is a good measure for assessing spin-isospin properties in the effective Hamiltonian. Applying a simple two-body interaction

$$V = \sum_{i<j} (\kappa_\tau \boldsymbol{\tau}_i \cdot \boldsymbol{\tau}_j + \kappa_\sigma \boldsymbol{\sigma}_i \cdot \boldsymbol{\sigma}_j + \kappa_{\sigma\tau} \boldsymbol{\tau}_i \cdot \boldsymbol{\tau}_j \boldsymbol{\sigma}_i \cdot \boldsymbol{\sigma}_j) \tag{32}$$

to a simple configuration in which excess neutrons occupy only a single j orbital, one obtains

$$E_{\rm GT} - E_{\rm IAS} = \Delta E_{ls} + 4(\kappa_{\sigma\tau} - \kappa_{\tau})T_0 \tag{33}$$

[12,69,71], where ΔE_{ls} denotes the spin-orbit splitting.

The first term of Eq. (33), ΔE_{ls}, is estimated to be $\approx 20A^{-1/3}$ MeV by using the empirical spin-orbit potential $-20(\boldsymbol{l}\cdot\boldsymbol{s})A^{-2/3}$ MeV [72] which leads to $\Delta E_{ls} = 20(l + 1/2)A^{-2/3} \approx 20A^{-1/3}$ MeV by substituting $l + 1/2 \approx A^{1/3}$ [69]. This quantity is consistent with that of Eq. (31), $17A^{-1/3}$ MeV. The actual spin-orbit splitting energies given by the present shell-model interaction are 6.3 and 5.1 MeV for the proton $1d$ and $1f$ orbitals, respectively, on top of the ^{42}Si core. These values are close to the first term of Eq. (30), 5.1 MeV.

The second term of Eq. (33), $4(\kappa_{\sigma\tau} - \kappa_{\tau})T_0$, indicates that the T_0 dependence of $E_{\rm GT} - E_{\rm IAS}$ is determined by the coupling constants of spin-isospin dependent forces. The fact that the corresponding terms in Eqs. (30) and (31) are close to the one of Eq. (27) may indicate that the effective coupling constants, apart from their mass dependence, are rather universal over the whole chart of nuclides.

Finally, we comment on a systematic deviation caused by the systematics. Taking a close look at Fig. 11, one can recognize that Eqs. (30) and (31) overestimate the shell-model values for smaller-Z isotopes and underestimate them for larger-Z isotopes as a whole. The deviation is enlarged when the systematics of Eq. (31) is used. This may be puzzling because the $A^{-1/3}$ dependence in Eq. (31) has a microscopic basis as mentioned above. What is missing in deriving the systematics is the evolution of the spin-orbit splitting due to the tensor force [73]. The tensor force causes local increase or decrease of the spin-orbit splitting depending on the occupancy of the $j_<$ or $j_>$ orbital. In the present case, in going from $Z = 14$ to 20, the proton $1d_{3/2}$ orbital is filled, as well as $2s_{1/2}$. The resulting spin-orbit splitting for the proton $1f$ orbitals is enlarged by approximately 1.5 MeV. In contrast, the ΔE_{ls} term is constant in Eq. (30) or even smoothly decreases with A in Eq. (31), thus causing a systematic deviation. Since the effect of the tensor force cannot be simply formulated in terms of proton and neutron numbers, any kind of functional formula has a limited descriptive power.

V. SUMMARY

We have performed a systematic shell-model study of β-decay half-lives and β-delayed neutron emission probabilities for neutron-rich nuclei with $13 \leqslant Z \leqslant 18$ and $22 \leqslant N \leqslant 34$. The valence shell consists of the full $sd + pf + sdg$ shell, and the effective interaction is the SDPF-MU interaction that is extended to the $sd + pf + sdg$ shell. The ground states are reasonably assumed to be the $0\hbar\omega$ states. For the Gamow-Teller (GT) transition, the final states are unnatural-parity states for the nuclei considered, and they are calculated in the $1\hbar\omega$ space within the valence shell taken. We have also evaluated the contributions of the first-forbidden (FF) transitions. The calculated β-decay half-lives and β-delayed neutron emission probabilities are in good agreement with the experimental data, as displayed by a quantitative error analysis. The calculations show that the FF transitions play a non-negligible role in the half-lives of $N \gtrsim 28$ nuclei.

Since the GT strengths obtained in this study satisfy the GT sum rule, we are able to investigate the GT strength distribution up to high excitation energies, including the GT giant resonance (GTGR). From the systematics of the calculated GT strength distributions, the following properties are obtained. (i) As the neutron number increases, the GTGR well develops. The GTGR carries most of the GT strengths, and the low-lying strengths decrease in accordance with the development of the GTGR. (ii) There is a strong even-odd effect in the low-lying GT strengths. Namely, the strengths from even-even nuclei are much more enhanced than the ones from the neighboring odd-A and odd-odd nuclei. The proton-neutron pairing interaction plays a dominant role in the formation of the enhanced strengths. (iii) The calculated positions of the GTGR are well formulated by a linear expression of $T_0 = (N - Z)/2$. Of particular interest is that the position of the GTGR can be located below that of the isobaric analog state, unlike what was observed in stable nuclei. The constant term obtained is somewhat different from that of the formula previously known, indicating that the average spin-orbit splitting does not change in a simple manner, influenced by the tensor force, for instance. These properties strongly influence the β-decay half-lives and β-delayed neutron emission probabilities. Hence, it is of great interest to further investigate how those properties are realized in other regions of the nuclear chart for a better understanding of the GT strength distribution, thus improving β-decay calculations.

ACKNOWLEDGMENTS

We thank C. Yuan for checking the code for calculating FF matrix elements. This work was supported in part by JSPS KAKENHI (Grants No. 15K05094, No. 17J06775, and No. 17K05433), by "Priority Issue 9 to be Tackled by Using Post-K Computer," and by the CNS-RIKEN joint project for large-scale nuclear structure calculations. The numerical calculations were performed with the BX900 and ICE X supercomputers at the Japan Atomic Energy Agency, and with Oakforest-PACS of JCAHPC through the HPCI System Research Project (Project ID: hp170182).

APPENDIX: TABULATED β-DECAY HALF-LIVES AND β-DELAYED NEUTRON EMISSION PROBABILITIES

The calculated values are compared to the experimental data in Tables IV, V, and VI.

TABLE IV. β-decay half-lives ($T_{1/2}$) and β-delayed neutron emission probabilities (P_n) in Al and Si isotopes compared between theory and experiment. The calculated values including the GT+FF contributions and the ones including only the GT contributions are denoted as full and GT, respectively. The $Q(\beta^-)$ values are taken from the AME2016 database [40] (exp.Q) which includes the values derived from systematic trends (marked with #), or the shell-model calculations (theo.Q). For the isotopes whose ground-state spin-parity quantum numbers are unknown, some candidates for the ground state are shown, together with their spin-parity and calculated excitation energies. The uncertainties in the experimental data refer to the last digits of the values, following the notation of ENSDF [46]; 37.2 ms 8 stands for 37.2 ± 0.8 ms, for instance.

Parent	$T_{1/2}$				P_n (%)			
	Exp.	Theory			Exp.	Theory		
	[46]	full (exp.Q)	full (theo.Q)	GT (theo.Q)	[46]	full (exp.Q)	full (theo.Q)	GT (theo.Q)
^{35}Al ($5/2^+$; g.s.)	37.2 ms 8	21.5 ms	14.2 ms	14.2 ms	38 2	25.4	22.0	22.0
^{36}Al (4^-; g.s.)	90 ms 40	14.4 ms	11.3 ms	11.4 ms		33.3	34.4	34.3
^{36}Al (2^-; 78 keV)	90 ms 40	17.1 ms	12.8 ms	12.9 ms		35.3	35.9	35.9
^{36}Al (1^-; 223 keV)	90 ms 40	16.9 ms	12.0 ms	12.1 ms		36.2	38.5	38.2
^{36}Al (5^-; 330 keV)	90 ms 40	15.3 ms	10.6 ms	10.6 ms		29.1	31.8	31.7
^{37}Al ($5/2^+$; g.s.)	10.7 ms 13	11.4 ms	9.06 ms	9.15 ms		46.0	48.1	48.0
^{38}Al (0^-; g.s.)	7.6 ms 6	8.66 ms	7.71 ms	8.01 ms		57.9	58.3	59.8
^{38}Al (5^-; 391 keV)	7.6 ms 6	8.47 ms	6.60 ms	6.65 ms		49.6	51.8	52.1
^{39}Al ($5/2^+$; g.s.)	7.6 ms 16	7.08 ms #	5.10 ms	5.35 ms		60.1 #	62.5	64.3
^{40}Al (4^-; g.s.)		5.84 ms #	3.39 ms	3.66 ms		49.0 #	55.0	59.1
^{40}Al (2^-; 179 keV)		6.05 ms #	3.31 ms	3.66 ms		53.3 #	58.4	63.9
^{40}Al (3^-; 301 keV)		7.43 ms #	3.80 ms	4.25 ms		67.6 #	71.7	79.2
^{40}Al (0^-; 362 keV)		5.68 ms #	2.89 ms	3.09 ms		93.5 #	95.1	99.6
^{40}Al (1^-; 448 keV)		5.70 ms #	2.83 ms	3.26 ms		76.3 #	79.4	90.3
^{41}Al ($5/2^+$; g.s.)		3.61 ms #	2.30 ms	2.84 ms		59.7 #	62.5	73.5
^{42}Al (3^-; g.s.)		6.32 ms #	1.86 ms	2.33 ms		98.7 #	84.9	96.1
^{42}Al (2^-; 105 keV)		6.49 ms #	1.84 ms	2.28 ms		97.3 #	82.6	88.9
^{42}Al (1^-; 251 keV)		5.95 ms #	1.64 ms	2.11 ms		98.0 #	91.1	97.2
^{42}Al (0^-; 337 keV)		6.42 ms #	1.71 ms	2.28 ms		98.5 #	86.1	98.5
^{42}Al (4^-; 344 keV)		8.90 ms #	2.24 ms	2.49 ms		99.4 #	91.7	92.7
^{43}Al ($5/2^+$; g.s.)		2.71 ms #	1.64 ms	2.07 ms		94.9 #	100	100
^{44}Al (2^-; g.s.)			1.27 ms	1.65 ms			95.4	100
^{44}Al (4^-; 80 keV)			1.36 ms	1.70 ms			99.8	100
^{44}Al (1^-; 181 keV)			1.12 ms	1.66 ms			80.7	100
^{44}Al (3^-; 267 keV)			1.19 ms	1.53 ms			97.7	100
^{45}Al ($5/2^+$; g.s.)			1.02 ms	1.37 ms			100	100
^{46}Al (2^-; g.s.)			0.816 ms	1.18 ms			97.1	100
^{46}Al (3^-; 248 keV)			0.763 ms	1.08 ms			97.9	100
^{47}Al ($5/2^+$; g.s.)			0.571 ms	0.881 ms			100	100
^{36}Si (0^+; g.s.)	0.45 s 6	0.340 s	0.334 s	0.335 s	12 5	3.6	4.1	4.1
^{37}Si ($5/2^-$; g.s.)	90 ms 60	115 ms	107 ms	110 ms	17 13	6.2	3.5	3.5
^{38}Si (0^+; g.s.)		82.0 ms	65.6 ms	66.5 ms		18.6	11.8	11.9
^{39}Si ($5/2^-$; g.s.)	47.5 ms 20	32.8 ms	28.3 ms	29.5 ms		20.1	19.4	20.2
^{39}Si ($7/2^-$; 44 keV)	47.5 ms 20	40.2 ms	33.6 ms	34.4 ms		23.3	22.7	23.2
^{39}Si ($3/2^-$; 98 keV)	47.5 ms 20	37.8 ms	30.8 ms	33.8 ms		30.9	29.5	32.4
^{40}Si (0^+; g.s.)	33.0 ms 10	25.1 ms	21.7 ms	22.6 ms		29.6	30.6	31.6
^{41}Si ($3/2^-$; g.s.)	20.0 ms 25	15.6 ms	12.7 ms	13.4 ms		53.3	49.8	52.9
^{42}Si (0^+; g.s.)	12.5 ms 35	9.05 ms #	9.67 ms	10.2 ms		38.2 #	37.7	36.7
^{43}Si ($3/2^-$; g.s.)		12.2 ms #	6.50 ms	7.70 ms		81.0 #	78.8	93.2
^{43}Si ($1/2^-$; 47 keV)		9.76 ms #	5.18 ms	6.21 ms		82.6 #	75.9	89.9
^{44}Si (0^+; g.s.)		7.85 ms #	5.11 ms	6.54 ms		81.5 #	83.7	100
^{45}Si ($1/2^-$; g.s.)		4.05 ms #	3.08 ms	4.58 ms		73.1 #	74.3	100
^{45}Si ($3/2^-$; 116 keV)		5.04 ms #	3.66 ms	5.47 ms		75.0 #	76.3	100
^{46}Si (0^+; g.s.)			2.58 ms	4.23 ms			93.4	100
^{47}Si ($1/2^-$; g.s.)			1.67 ms	3.45 ms			71.5	100
^{48}Si (0^+; g.s.)			1.13 ms	2.42 ms			96.0	100

TABLE V. Same as Table IV but for P and S isotopes.

Parent	$T_{1/2}$				P_n (%)			
	Exp.	Theory			Exp.	Theory		
	[46]	full (exp.Q)	full (theo.Q)	GT (theo.Q)	[46]	full (exp.Q)	full (theo.Q)	GT (theo.Q)
^{37}P ($1/2^+$; g.s.)	2.31 s 13	1.66 s	1.92 s	1.93 s		6.2	4.4	4.4
^{38}P (2^-; g.s.)	0.64 s 14	0.315 s	0.405 s	0.428 s	12 5	3.9	2.7	2.9
^{38}P (1^-; 158 keV)	0.64 s 14	0.351 s	0.407 s	0.423 s	12 5	4.8	3.6	3.8
^{38}P (3^-; 284 keV)	0.64 s 14	0.478 s	0.511 s	0.526 s	12 5	5.4	4.6	4.7
^{38}P (4^-; 421 keV)	0.64 s 14	0.415 s	0.404 s	0.413 s	12 5	5.8	5.2	5.3
^{39}P ($1/2^+$; g.s.)	0.28 s 4	0.289 s	0.239 s	0.246 s	26 8	21.8	22.6	23.2
^{40}P (2^-; g.s.)	150 ms 8	121 ms	105 ms	113 ms	15.8 21	19.6	21.1	22.8
^{40}P (3^-; 321 keV)	150 ms 8	163 ms	118 ms	125 ms	15.8 21	22.3	25.3	26.8
^{41}P ($1/2^+$; g.s.)	101 ms 5	93.1 ms	72.4 ms	77.3 ms	30 10	39.1	42.4	44.2
^{42}P (0^-; g.s.)	48.5 ms 15	30.7 ms	25.6 ms	41.9 ms	50 20	29.5	32.3	51.8
^{42}P (1^-; 133 keV)	48.5 ms 15	41.7 ms	33.3 ms	41.9 ms	50 20	43.7	47.4	58.9
^{42}P (2^-; 188 keV)	48.5 ms 15	49.5 ms	39.4 ms	45.9 ms	50 20	50.3	55.1	64.1
^{42}P (3^-; 290 keV)	48.5 ms 15	56.9 ms	39.3 ms	41.4 ms	50 20	64.4	72.2	76.0
^{42}P (4^-; 413 keV)	48.5 ms 15	62.3 ms	40.5 ms	41.6 ms	50 20	73.2	79.9	82.1
^{43}P ($1/2^+$; g.s.)	36.5 ms 15	29.6 ms	25.6 ms	29.1 ms	100	93.6	93.8	98.3
^{44}P (0^-; g.s.)	18.5 ms 25	18.9 ms #	13.0 ms	16.9 ms		75.0 #	78.8	98.0
^{44}P (1^-; 267 keV)	18.5 ms 25	21.9 ms #	12.9 ms	16.6 ms		74.7 #	76.9	97.1
^{44}P (2^-; 352 keV)	18.5 ms 25	27.7 ms #	16.0 ms	19.4 ms		73.0 #	77.9	92.8
^{45}P ($1/2^+$; g.s.)		11.2 ms #	10.8 ms	14.8 ms		78.3 #	79.1	100
^{46}P (0^-; g.s.)		7.74 ms #	6.34 ms	10.5 ms		65.9 #	68.3	100
^{46}P (2^-; 151 keV)		11.0 ms #	8.33 ms	12.3 ms		73.9 #	76.1	100
^{46}P (1^-; 473 keV)		9.40 ms #	6.50 ms	9.54 ms		75.7 #	78.6	100
^{47}P ($1/2^+$; g.s.)		4.08 ms #	5.09 ms	8.47 ms		82.9 #	80.6	100
^{48}P (0^-; g.s.)			3.47 ms	7.83 ms			65.1	100
^{48}P (1^-; 388 keV)			3.09 ms	6.21 ms			69.1	100
^{49}P ($1/2^+$; g.s.)			2.02 ms	4.24 ms			80.2	100
^{38}S (0^+; g.s.)	170.3 min 7	72.1 min	24.1 min	25.6 min				
^{39}S ($3/2^-$; g.s.)	11.5 s 5	13.6 s	14.7 s	15.8 s				
^{39}S ($5/2^-$; 137 keV)	11.5 s 5	13.4 s	12.0 s	12.3 s				
^{39}S ($7/2^-$; 188 keV)	11.5 s 5	18.2 s	15.1 s	15.4 s				
^{40}S (0^+; g.s.)	8.8 s 22	13.3 s	6.41 s	6.45 s				
^{41}S ($5/2^-$; g.s.)	1.99 s 5	1.86 s	1.52 s	1.55 s				
^{42}S (0^+; g.s.)	1.016 s 15	1.27 s	0.789 s	0.796 s		0.1	0.2	0.2
^{43}S ($3/2^-$; g.s.)	265 ms 15	290 ms	227 ms	248 ms	40 10	7.8	10.6	11.6
^{43}S ($1/2^-$; 135 keV)	265 ms 15	146 ms	110 ms	115 ms	40 10	2.5	4.6	4.8
^{44}S (0^+; g.s.)	100 ms 1	114 ms	82.0 ms	86.8 ms	18 3	16.7	19.0	20.0
^{45}S ($3/2^-$; g.s.)	68 ms 2	90.5 ms	44.4 ms	49.4 ms	54	30.5	50.8	56.6
^{45}S ($1/2^-$; 239 keV)	68 ms 2	73.6 ms	33.1 ms	37.8 ms	54	30.7	48.5	55.4
^{46}S (0^+; g.s.)	50 ms 8	36.2 ms #	28.3 ms	31.3 ms		84.5 #	93.4	100
^{47}S ($1/2^-$; g.s.)		18.9 ms #	12.8 ms	16.0 ms		73.4 #	65.1	79.7
^{47}S ($3/2^-$; 73 keV)		26.4 ms #	17.2 ms	21.4 ms		77.3 #	78.9	97.6
^{48}S (0^+; g.s.)		10.7 ms #	11.5 ms	14.7 ms		82.3 #	82.2	100
^{49}S ($1/2^-$; g.s.)		7.92 ms #	8.06 ms	12.3 ms		84.4 #	68.4	100
^{50}S (0^+; g.s.)			4.95 ms	7.22 ms			88.8	100

TABLE VI. Same as Table IV but for Cl and Ar isotopes.

Parent	$T_{1/2}$				P_n (%)			
	Exp.	Theory			Exp.	Theory		
	[46]	full (exp.Q)	full (theo.Q)	GT (theo.Q)	[46]	full (exp.Q)	full (theo.Q)	GT (theo.Q)
^{39}Cl ($3/2^+$; g.s.)	56.2 min 6	17.9 min	13.6 min	13.9 min				
^{40}Cl (2^-; g.s.)	1.35 min 3	0.569 min	0.864 min	1.08 min				
^{40}Cl (1^-; 30 keV)	1.35 min 3	0.576 min	0.852 min	0.919 min				
^{41}Cl ($1/2^+$; g.s.)	38.4 s 8	30.6 s	16.0 s	16.1 s				
^{42}Cl (2^-; g.s.)	6.8 s 3	5.49 s	5.49 s	5.75 s				
^{42}Cl (3^-; 153 keV)	6.8 s 3	4.56 s	3.96 s	4.05 s				
^{43}Cl ($1/2^+$; g.s.)	3.13 s 9	4.51 s	2.20 s	2.28 s		2.9	2.0	2.1
^{43}Cl ($3/2^+$; 269 keV)	3.13 s 9	6.30 s	2.25 s	2.33 s		3.2	5.3	5.5
^{44}Cl (2^-; g.s.)	0.56 s 11	0.614 s	0.478 s	0.679 s		2.5	6.2	8.8
^{45}Cl ($1/2^+$; g.s.)	413 ms 25	293 ms	179 ms	196 ms	24 4	13.7	15.8	17.1
^{46}Cl (0^-; g.s.)	232 ms 2	230 ms	124 ms	166 ms	60 9	29.3	39.3	50.9
^{46}Cl (2^-; 161 keV)	232 ms 2	221 ms	110 ms	131 ms	60 9	21.7	34.1	40.6
^{46}Cl (1^-; 313 keV)	232 ms 2	208 ms	94.4 ms	108 ms	60 9	22.1	33.4	37.6
^{46}Cl (3^-; 369 keV)	232 ms 2	311 ms	131 ms	156 ms	60 9	30.4	48.7	57.8
^{47}Cl ($1/2^+$; g.s.)	101 ms 6	85.7 ms #	56.9 ms	69.1 ms		84.2 #	86.4	100
^{47}Cl ($3/2^+$; 33 keV)	101 ms 6	106 ms #	68.6 ms	83.6 ms		75.0 #	86.9	100
^{48}Cl (2^-; g.s.)		63.7 ms #	35.1 ms	50.9 ms		61.3 #	71.4	98.7
^{48}Cl (3^-; 58 keV)		85.7 ms #	43.1 ms	57.7 ms		73.9 #	78.7	98.1
^{48}Cl (0^-; 78 keV)		29.4 ms #	18.3 ms	37.9 ms		38.1 #	50.3	100
^{48}Cl (1^-; 119 keV)		53.2 ms #	27.2 ms	40.3 ms		63.8 #	71.6	100
^{49}Cl ($3/2^+$; g.s.)		26.3 ms #	24.7 ms	34.2 ms		82.5 #	82.5	100
^{50}Cl (2^-; g.s.)		16.1 ms #	14.4 ms	19.8 ms		87.0 #	87.5	100
^{50}Cl (1^-; 134 keV)		15.8 ms #	13.5 ms	21.4 ms		75.0 #	77.2	100
^{51}Cl ($3/2^+$; g.s.)		7.45 ms #	7.61 ms	10.5 ms		95.5 #	94.7	100
^{41}Ar ($5/2^-$; g.s.)	109.61 min 4	94.4 min	1.68e+03 min	1.73e+03 min				
^{41}Ar ($7/2^-$; 279 keV)	109.61 min 4	206 min	754 min	768 min				
^{42}Ar (0^+; g.s.)	32.9 y 11	66.5 y	6.39 y					
^{43}Ar ($5/2^-$; g.s.)	5.37 min 6	3.03 min	6.43 min	7.74 min				
^{43}Ar ($7/2^-$; 124 keV)	5.37 min 6	3.16 min	5.03 min	5.14 min				
^{43}Ar ($3/2^-$; 336 keV)	5.37 min 6	2.66 min	2.68 min	4.79 min				
^{44}Ar (0^+; g.s.)	11.87 min 5	8.02 min	3.31 min	3.35 min				
^{45}Ar ($7/2^-$; g.s.)	21.48 s 15	9.84 s	12.2 s	12.4 s				
^{45}Ar ($3/2^-$; 316 keV)	21.48 s 15	13.7 s	11.4 s	16.0 s				
^{46}Ar (0^+; g.s.)	8.4 s 6	6.65 s	5.25 s	5.30 s				
^{47}Ar ($3/2^-$; g.s.)	1.23 s 3	1.47 s	0.856 s	0.921 s		0.6	1.3	1.4
^{48}Ar (0^+; g.s.)	475 ms 40	353 ms	298 ms	307 ms		20.2	29.7	30.4
^{49}Ar ($3/2^-$; g.s.)	170 ms 50	274 ms #	161 ms	189 ms	65 20	47.0 #	51.6	60.5
^{50}Ar (0^+; g.s.)	106 ms 6	120 ms #	82.9 ms	95.8 ms	35 10	39.7 #	44.9	51.8
^{51}Ar ($1/2^-$; g.s.)		38.3 ms #	32.7 ms	44.3 ms		58.4 #	65.6	87.6
^{52}Ar (0^+; g.s.)		17.5 ms #	14.7 ms	17.3 ms		86.9 #	100	100

[1] S. Nishimura, Z. Li, H. Watanabe, K. Yoshinaga, T. Sumikama, T. Tachibana, K. Yamaguchi, M. Kurata-Nishimura, G. Lorusso, Y. Miyashita, A. Odahara, H. Baba, J. S. Berryman, N. Blasi, A. Bracco, F. Camera, J. Chiba, P. Doornenbal, S. Go, T. Hashimoto,

S. Hayakawa, C. Hinke, E. Ideguchi, T. Isobe, Y. Ito, D. G. Jenkins, Y. Kawada, N. Kobayashi, Y. Kondo, R. Krücken, S. Kubono, T. Nakano, H. J. Ong, S. Ota, Z. Podolyák, H. Sakurai, H. Scheit, K. Steiger, D. Steppenbeck, K. Sugimoto, S. Takano, A. Takashima, K. Tajiri, T. Teranishi, Y. Wakabayashi, P. M. Walker, O. Wieland, and H. Yamaguchi, Phys. Rev. Lett. **106**, 052502 (2011).

[2] R. Caballero-Folch, C. Domingo-Pardo, J. Agramunt, A. Algora, F. Ameil, A. Arcones, Y. Ayyad, J. Benlliure, I. N. Borzov, M. Bowry, F. Calviño, D. Cano-Ott, G. Cortés, T. Davinson, I. Dillmann, A. Estrade, A. Evdokimov, T. Faestermann, F. Farinon, D. Galaviz, A. R. García, H. Geissel, W. Gelletly, R. Gernhäuser, M. B. Gómez-Hornillos, C. Guerrero, M. Heil, C. Hinke, R. Knöbel, I. Kojouharov, J. Kurcewicz, N. Kurz, Y. A. Litvinov, L. Maier, J. Marganiec, T. Marketin, M. Marta, T. Martínez, G. Martínez-Pinedo, F. Montes, I. Mukha, D. R. Napoli, C. Nociforo, C. Paradela, S. Pietri, Z. Podolyák, A. Prochazka, S. Rice, A. Riego, B. Rubio, H. Schaffner, C. Scheidenberger, K. Smith, E. Sokol, K. Steiger, B. Sun, J. L. Taín, M. Takechi, D. Testov, H. Weick, E. Wilson, J. S. Winfield, R. Wood, P. Woods, and A. Yeremin, Phys. Rev. Lett. **117**, 012501 (2016).

[3] M. Madurga, R. Surman, I. N. Borzov, R. Grzywacz, K. P. Rykaczewski, C. J. Gross, D. Miller, D. W. Stracener, J. C. Batchelder, N. T. Brewer, L. Cartegni, J. H. Hamilton, J. K. Hwang, S. H. Liu, S. V. Ilyushkin, C. Jost, M. Karny, A. Korgul, W. Królas, A. Kuźniak, C. Mazzocchi, A. J. Mendez, K. Miernik, S. W. Padgett, S. V. Paulauskas, A. V. Ramayya, J. A. Winger, M. Wolińska-Cichocka, and E. F. Zganjar, Phys. Rev. Lett. **109**, 112501 (2012).

[4] J. Pereira, S. Hennrich, A. Aprahamian, O. Arndt, A. Becerril, T. Elliot, A. Estrade, D. Galaviz, R. Kessler, K.-L. Kratz, G. Lorusso, P. F. Mantica, M. Matos, P. Möller, F. Montes, B. Pfeiffer, H. Schatz, F. Schertz, L. Schnorrenberger, E. Smith, A. Stolz, M. Quinn, W. B. Walters, and A. Wöhr, Phys. Rev. C **79**, 035806 (2009).

[5] S. Grévy, J. Angélique, P. Baumann, C. Borcea, A. Buta, G. Canchel, W. Catford, S. Courtin, J. Daugas, F. de Oliveira, P. Dessagne, Z. Dlouhy, A. Knipper, K. Kratz, F. Lecolley, J. Lecouey, G. Lehrsenneau, M. Lewitowicz, E. Liénard, S. Lukyanov, F. Maréchal, C. Miehé, J. Mrazek, F. Negoita, N. Orr, D. Pantelica, Y. Penionzhkevich, J. Péter, B. Pfeiffer, S. Pietri, E. Poirier, O. Sorlin, M. Stanoiu, I. Stefan, C. Stodel, and C. Timis, Phys. Lett. B **594**, 252 (2004).

[6] R. Dunlop, V. Bildstein, I. Dillmann, A. Jungclaus, C. E. Svensson, C. Andreoiu, G. C. Ball, N. Bernier, H. Bidaman, P. Boubel, C. Burbadge, R. Caballero-Folch, M. R. Dunlop, L. J. Evitts, F. Garcia, A. B. Garnsworthy, P. E. Garrett, G. Hackman, S. Hallam, J. Henderson, S. Ilyushkin, D. Kisliuk, R. Krücken, J. Lassen, R. Li, E. MacConnachie, A. D. MacLean, E. McGee, M. Moukaddam, B. Olaizola, E. Padilla-Rodal, J. Park, O. Paetkau, C. M. Petrache, J. L. Pore, A. J. Radich, P. Ruotsalainen, J. Smallcombe, J. K. Smith, S. L. Tabor, A. Teigelhöfer, J. Turko, and T. Zidar, Phys. Rev. C **93**, 062801 (2016).

[7] H. Koura and S. Chiba, Phys. Rev. C **95**, 064304 (2017).

[8] P. Möller, B. Pfeiffer, and K.-L. Kratz, Phys. Rev. C **67**, 055802 (2003), see also the data file at http://t2.lanl.gov/nis/molleretal/publications/rspeed2002.html

[9] T. Marketin, L. Huther, and G. Martínez-Pinedo, Phys. Rev. C **93**, 025805 (2016).

[10] M. Arnould, S. Goriely, and K. Takahashi, Phys. Rep. **450**, 97 (2007).

[11] M. T. Mustonen and J. Engel, Phys. Rev. C **93**, 014304 (2016).

[12] F. Osterfeld, Rev. Mod. Phys. **64**, 491 (1992).

[13] T. Nakamura, T. Aumann, D. Bazin, Y. Blumenfeld, B. Brown, J. Caggiano, R. Clement, T. Glasmacher, P. Lofy, A. Navin, B. Pritychenko, B. Sherrill, and J. Yurkon, Phys. Lett. B **493**, 209 (2000).

[14] R. G. T. Zegers, R. Meharchand, Y. Shimbara, S. M. Austin, D. Bazin, B. A. Brown, C. A. Diget, A. Gade, C. J. Guess, M. Hausmann, G. W. Hitt, M. E. Howard, M. King, D. Miller, S. Noji, A. Signoracci, K. Starosta, C. Tur, C. Vaman, P. Voss, D. Weisshaar, and J. Yurkon, Phys. Rev. Lett. **104**, 212504 (2010).

[15] Y. Satou, T. Nakamura, Y. Kondo, N. Matsui, Y. Hashimoto, T. Nakabayashi, T. Okumura, M. Shinohara, N. Fukuda, T. Sugimoto, H. Otsu, Y. Togano, T. Motobayashi, H. Sakurai, Y. Yanagisawa, N. Aoi, S. Takeuchi, T. Gomi, M. Ishihara, S. Kawai, H. Ong, T. Onishi, S. Shimoura, M. Tamaki, T. Kobayashi, Y. Matsuda, N. Endo, and M. Kitayama, Phys. Lett. B **697**, 459 (2011).

[16] M. Sasano, G. Perdikakis, R. G. T. Zegers, S. M. Austin, D. Bazin, B. A. Brown, C. Caesar, A. L. Cole, J. M. Deaven, N. Ferrante, C. J. Guess, G. W. Hitt, R. Meharchand, F. Montes, J. Palardy, A. Prinke, L. A. Riley, H. Sakai, M. Scott, A. Stolz, L. Valdez, and K. Yako, Phys. Rev. Lett. **107**, 202501 (2011).

[17] B. Brown and B. Wildenthal, At. Data Nucl. Data Tables **33**, 347 (1985).

[18] E. Caurier, G. Martínez-Pinedo, F. Nowacki, A. Poves, and A. P. Zuker, Rev. Mod. Phys. **77**, 427 (2005).

[19] M. Honma, T. Otsuka, T. Mizusaki, M. Hjorth-Jensen, and B. A. Brown, J. Phys.: Conf. Ser. **20**, 7 (2005).

[20] K. Langanke and G. Martínez-Pinedo, At. Data Nucl. Data Tables **79**, 1 (2001).

[21] H. Li and Z. Ren, J. Phys. G: Nucl. Part. Phys. **40**, 105110 (2013).

[22] T. Suzuki, T. Yoshida, T. Kajino, and T. Otsuka, Phys. Rev. C **85**, 015802 (2012).

[23] Q. Zhi, E. Caurier, J. J. Cuenca-García, K. Langanke, G. Martínez-Pinedo, and K. Sieja, Phys. Rev. C **87**, 025803 (2013).

[24] V. Kumar, P. C. Srivastava, and H. Li, J. Phys. G: Nucl. Part. Phys. **43**, 105104 (2016).

[25] See Supplemental Material at http://link.aps.org/supplemental/10.1103/PhysRevC.97.054321 for the detailed results of excitation spectra and B(GT) distributions.

[26] E. K. Warburton, J. A. Becker, and B. A. Brown, Phys. Rev. C **41**, 1147 (1990).

[27] Y. Utsuno, T. Otsuka, B. A. Brown, M. Honma, T. Mizusaki, and N. Shimizu, Prog. Theor. Phys. Suppl. **196**, 304 (2012).

[28] A. Gade, J. A. Tostevin, V. Bader, T. Baugher, D. Bazin, J. S. Berryman, B. A. Brown, D. J. Hartley, E. Lunderberg, F. Recchia, S. R. Stroberg, Y. Utsuno, D. Weisshaar, and K. Wimmer, Phys. Rev. C **93**, 031601 (2016).

[29] R. Whitehead, A. Watt, and D. Kelvin, Phys. Lett. B **89**, 313 (1980).

[30] R. R. Whitehead, in *Theory and Applications of Moment Methods in Many-Fermion Systems*, edited by B. J. Dalton, S. M. Grimes, J. P. Vary, and S. A. Williams (Springer, Boston, 1980), pp. 235–255.

[31] Y. Utsuno, T. Otsuka, B. A. Brown, M. Honma, T. Mizusaki, and N. Shimizu, Phys. Rev. C **86**, 051301 (2012).

[32] T. Otsuka, T. Suzuki, M. Honma, Y. Utsuno, N. Tsunoda, K. Tsukiyama, and M. Hjorth-Jensen, Phys. Rev. Lett. **104**, 012501 (2010).

[33] N. Shimizu, arXiv:1310.5431.

[34] J. C. Hardy and I. S. Towner, Phys. Rev. C **79**, 055502 (2009).

[35] J. Beringer *et al.* (Particle Data Group), Phys. Rev. D **86**, 010001 (2012).

[36] K. Ikeda, S. Fujii, and J. Fujita, Phys. Lett. **3**, 271 (1963).

[37] C. Gaarde, J. Larsen, M. Harakeh, S. van der Werf, M. Igarashi, and A. Müller-Arnke, Nucl. Phys. A **334**, 248 (1980).

[38] J. Duflo and A. P. Zuker, Phys. Rev. C **52**, R23 (1995).

[39] E. Caurier, G. Martínez-Pinedo, F. Nowacki, A. Poves, J. Retamosa, and A. P. Zuker, Phys. Rev. C **59**, 2033 (1999).

[40] M. Wang, G. Audi, F. Kondev, W. Huang, S. Naimi, and X. Xu, Chin. Phys. C **41**, 030003 (2017).

[41] E. Warburton, J. Becker, B. Brown, and D. Millener, Ann. Phys. **187**, 471 (1988).

[42] H. Behrens and W. Bühring, Nucl. Phys. A **162**, 111 (1971).

[43] I. Towner and J. Hardy, in *Symmetries and Fundamental Interactions in Nuclei*, edited by W. Haxton and E. Henley (World Scientific, Singapore, 1995), p. 183.

[44] G. Martínez-Pinedo, A. Poves, E. Caurier, and A. P. Zuker, Phys. Rev. C **53**, R2602 (1996).

[45] F. Perrot, F. Maréchal, C. Jollet, P. Dessagne, J.-C. Angélique, G. Ban, P. Baumann, F. Benrachi, U. Bergmann, C. Borcea, A. Buţă, J. Cederkall, S. Courtin, J.-M. Daugas, L. M. Fraile, S. Grévy, A. Jokinen, F. R. Lecolley, E. Liénard, G. L. Scornet, V. Méot, C. Miehé, F. Negoiţă, N. A. Orr, S. Pietri, E. Poirier, M. Ramdhane, O. Roig, I. Stefan, and W. Wang, Phys. Rev. C **74**, 014313 (2006).

[46] ENSDF database, http://www.nndc.bnl.gov/ensdf/

[47] V. Tripathi, R. S. Lubna, B. Abromeit, H. L. Crawford, S. N. Liddick, Y. Utsuno, P. C. Bender, B. P. Crider, R. Dungan, P. Fallon, K. Kravvaris, N. Larson, A. O. Macchiavelli, T. Otsuka, C. J. Prokop, A. L. Richard, N. Shimizu, S. L. Tabor, A. Volya, and S. Yoshida, Phys. Rev. C **95**, 024308 (2017).

[48] P. Baumann, M. Bounajma, F. Didierjean, A. Huck, A. Knipper, M. Ramdhane, G. Walter, G. Marguier, C. Richard-Serre, and B. A. Brown, Phys. Rev. C **58**, 1970 (1998).

[49] J. Retamosa, E. Caurier, F. Nowacki, and A. Poves, Phys. Rev. C **55**, 1266 (1997).

[50] S. Nummela, P. Baumann, E. Caurier, P. Dessagne, A. Jokinen, A. Knipper, G. Le Scornet, C. Miehé, F. Nowacki, M. Oinonen, Z. Radivojevic, M. Ramdhane, G. Walter, and J. Äystö, Phys. Rev. C **63**, 044316 (2001).

[51] K. Steiger, S. Nishimura, Z. Li, R. Gernhäuser, Y. Utsuno, R. Chen, T. Faestermann, C. Hinke, R. Krücken, M. Kurata-Nishimura, G. Lorusso, Y. Miyashita, N. Shimizu, K. Sugimoto, T. Sumikama, H. Watanabe, and K. Yoshinaga, Eur. Phys. J. A **51**, 117 (2015).

[52] D. Verney, D. Testov, F. Ibrahim, Y. Penionzhkevich, B. Roussière, V. Smirnov, F. Didierjean, K. Flanagan, S. Franchoo, E. Kuznetsova, R. Li, B. Marsh, I. Matea, H. Pai, E. Sokol, I. Stefan, and D. Suzuki, Phys. Rev. C **95**, 054320 (2017).

[53] L. Weissman, U. Bergmann, J. Cederkall, L. Fraile, S. Franchoo, H. O. U. Fynbo, T. Fritioff, U. Koster, O. Arnd, I. Dillman, O. Hallmann, K.-L. Kratz, B. Pfeiffer, A. Wohr, L. Gaudefroy, O. Sorlin (ISOLDE Collaboration), J. Phys.: Conf. Ser. **337**, 012018 (2012).

[54] J. C. Hill, R. F. Petry, and K. H. Wang, Phys. Rev. C **21**, 384 (1980).

[55] J. A. Winger, P. F. Mantica, and R. M. Ronningen, Phys. Rev. C **73**, 044318 (2006).

[56] J. A. Winger, P. F. Mantica, R. M. Ronningen, and M. A. Caprio, Phys. Rev. C **64**, 064318 (2001).

[57] E. R. White, H. Mach, L. M. Fraile, U. Köster, O. Arndt, A. Blazhev, N. Boelaert, M. J. G. Borge, R. Boutami, H. Bradley, N. Braun, Z. Dlouhy, C. Fransen, H. O. U. Fynbo, C. Hinke, P. Hoff, A. Joinet, A. Jokinen, J. Jolie, A. Korgul, K.-L. Kratz, T. Kröll, W. Kurcewicz, J. Nyberg, E.-M. Reillo, E. Ruchowska, W. Schwerdtfeger, G. S. Simpson, M. Stanoiu, O. Tengblad, P. G. Thirolf, V. Ugryumov, and W. B. Walters, Phys. Rev. C **76**, 057303 (2007).

[58] A. Huck, G. Klotz, A. Knipper, C. Miehe, C. Richard-Serre, and G. Walter, in *4th International Conference on Nuclei Far from Stability*, Helsingør, *Denmark, 7–13 June 1981* (CERN, Geneva, 1981), pp. 378–386.

[59] K. Gurach, A. P. Kabachenko, I. V. Kuznetsov, and N. I. Tarantin, Yad. Fiz. **19**, 1167 (1974).

[60] J. Engel, M. Bender, J. Dobaczewski, W. Nazarewicz, and R. Surman, Phys. Rev. C **60**, 014302 (1999).

[61] Z. Niu, Y. Niu, H. Liang, W. Long, T. Nikšić, D. Vretenar, and J. Meng, Phys. Lett. B **723**, 172 (2013).

[62] K. Yoshida, Prog. Theor. Exp. Phys. **2013**, 113B02 (2013).

[63] C. Bai, H. Sagawa, M. Sasano, T. Uesaka, K. Hagino, H. Zhang, X. Zhang, and F. Xu, Phys. Lett. B **719**, 116 (2013).

[64] C. L. Bai, H. Sagawa, G. Colò, Y. Fujita, H. Q. Zhang, X. Z. Zhang, and F. R. Xu, Phys. Rev. C **90**, 054335 (2014).

[65] Y. Fujita, H. Fujita, T. Adachi, C. L. Bai, A. Algora, G. P. A. Berg, P. von Brentano, G. Colò, M. Csatlós, J. M. Deaven, E. Estevez-Aguado, C. Fransen, D. De Frenne, K. Fujita, E. Ganioğlu, C. J. Guess, J. Gulyás, K. Hatanaka, K. Hirota, M. Honma, D. Ishikawa, E. Jacobs, A. Krasznahorkay, H. Matsubara, K. Matsuyanagi, R. Meharchand, F. Molina, K. Muto, K. Nakanishi, A. Negret, H. Okamura, H. J. Ong, T. Otsuka, N. Pietralla, G. Perdikakis, L. Popescu, B. Rubio, H. Sagawa, P. Sarriguren, C. Scholl, Y. Shimbara, Y. Shimizu, G. Susoy, T. Suzuki, Y. Tameshige, A. Tamii, J. H. Thies, M. Uchida, T. Wakasa, M. Yosoi, R. G. T. Zegers, K. O. Zell, and J. Zenihiro, Phys. Rev. Lett. **112**, 112502 (2014).

[66] T. Tachibana, M. Yamada, and Y. Yoshida, Prog. Theor. Phys. **84**, 641 (1990).

[67] K. Ikeda, S. Fujii, and F. Fujita, Phys. Lett. **2**, 169 (1962).

[68] D. Horen, C. Goodman, D. Bainum, C. Foster, C. Gaarde, C. Goulding, M. Greenfield, J. Rapaport, T. Taddeucci, E. Sugarbaker, T. Masterson, S. Austin, A. Galonsky, and W. Sterrenburg, Phys. Lett. B **99**, 383 (1981).

[69] K. Nakayama, A. P. Galeão, and F. Krmpotić, Phys. Lett. B **114**, 217 (1982).

[70] K. Pham, J. Jänecke, D. A. Roberts, M. N. Harakeh, G. P. A. Berg, S. Chang, J. Liu, E. J. Stephenson, B. F. Davis, H. Akimune, and M. Fujiwara, Phys. Rev. C **51**, 526 (1995).

[71] S. Fracasso and G. Colò, Phys. Rev. C **76**, 044307 (2007).

[72] A. Bohr and B. Mottelson, *Nuclear Structure: Volume 1, Single-Particle Motion* (Benjamin, New York, 1969).

[73] T. Otsuka, T. Suzuki, R. Fujimoto, H. Grawe, and Y. Akaishi, Phys. Rev. Lett. **95**, 232502 (2005).